

Experimental Determination of Transfer Functions for a Coated, Ring Stiffened Cylinder as a Function of Hydrostatic Pressure

by

Robert H. Meyer

B.S.N.E. The Pennsylvania State University (1986)

Submitted to the Department of Ocean Engineering
and the Department of Mechanical Engineering
in Partial Fulfillment of the Requirements for the Degrees of

Naval Engineer
and

Master of Science in Mechanical Engineering

at the

MASSACHUSETTS INSTITUTE OF TECHNOLOGY

June 1997

©1997 Robert H. Meyer

All rights reserved

The Author hereby grants to MIT permission to reproduce and to distribute publicly
paper and electronic copies of this thesis in whole or in part.

Signature of Author

Robert H. Meyer
Department of Ocean Engineering
May 12, 1997

Certified by

Henrik Schmidt
Henrik Schmidt
Professor of Ocean Engineering
Thesis Supervisor

Certified by

James H. Williams, Jr.
James H. Williams, Jr.
Professor of Mechanical Engineering
Thesis Supervisor

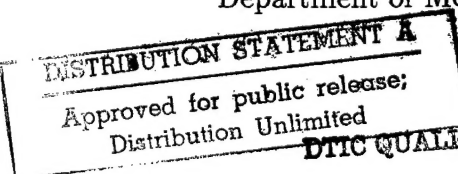
Accepted by

J. Kim Vandiver
J. Kim Vandiver
Chairman, Committee on Graduate Students
Department of Ocean Engineering

Accepted by

Ain Ants Sonin
Ain Ants Sonin
Chairman, Committee on Graduate Students
Department of Mechanical Engineering

19970703 070



DTIC QUALITY INSPECTED 1

Experimental determination of the transfer functions for a coated, ring stiffened cylinder as a function of hydrostatic pressure

by Robert H. Meyer

Submitted to the Department of Ocean Engineering and the Department of Mechanical Engineering on May 12, 1997, in partial fulfillment of the requirements for the degrees of Naval Engineer and Master of Science in Mechanical Engineering

Abstract

Coating effectiveness, as measured by the change in a ring stiffened cylinder's transfer function, is experimentally determined in the acoustic far field for increasing hydrostatic pressure. Polymer coating response characteristics are a function of temperature, frequency, molecular structure, chemical cross-linking systems and fillers. A sample coating, of unknown composition, is provided for analysis to gage performance as a function of frequency and filler (indirectly through hydrostatic pressure). Limited instrumentation assets (16 channels) required a pre-lake structural test program. Results of this test program determined the shell placement of accelerometers channels and provided an evaluation of bulkhead and shell radiated power levels. Results were highly subjective to boundary conditions and close proximity of nodal / resonant points thereby making 1/6 th octave sampling unsuitable for the lake test program

Deep water testing was conducted at the Acoustic Research Detachment, Pend Oreille, Idaho between 3 to 12 March 1997. The far field power levels were measured using an equally spaced 5 element line array placed 25 feet from the cylinder's beam. Measurements were made for 3 operating depths; 50 ft, 200 ft and 450 ft. Twenty one frequency bins using an LFM sweep over a pass band of 400 Hz to 10.5 kHz were digitized then analyzed using MATLAB. Results show a 7 to 8 dB reduction at 50 feet; 3-5 dB at 200 feet and 3 dB for the maximum 450 foot depth. For each depth, the reduction in hull excitation was greater than far field leading to an increase in transfer function even though far field is reduced. Decay of excitation with distance from forcing points is significant for bare hull and much more rapid for a coated hull.

Thesis Supervisor: Dr. Henrik Schmidt
Title: Professor of Ocean Engineering

Thesis Reader: Dr. James H. Williams, Jr.
Title: Professor of Mechanical Engineering

Acknowledgments:

Acknowledgments can be like thanking the people who got you in the position to win an Oscar. The question, invariably, becomes who do you thank without leaving someone out.

First, I would like to thank my partners in this scientific effort, Dr. Ron Dicus and Mr. Vijay Kohli both of Science Applications International Corporation (SAIC). Along with my thesis advisor, Professor Henrik Schmidt, they provided the inspiration to tackle this problem. I only wish that I could learn more from these giants in the field of acoustics.

The fact that I had the opportunity to even work with these people can be attributed to my sponsor, Mr. John Thomas of Naval Sea Systems Command. John came up with the original idea of studying the effects of hydrostatic pressure on coating performance. With only this idea and having very little money, I was able to convince Mr. Stan Siegel of the Advanced Projects Administration (ARPA) to lend me his very expensive test section. The price of this loan was simply to forward a copy of this thesis when it was completed. I wish all my negotiations were this simple. The pre-lake test program was conducted at Draper Labs. Like SAIC, Draper is a talented organization because of people like Pete Sebelius, Alex Edsall and Chris Dafnoulelis.

But the fact that I made it through, at all, can only be attributed to support that I continue to get from my family. Being a navy man, my wife Heidi has seen me leave on more than a few deployments. But unlike sea duty where you know that your husband is not going to be there for the next few months, she made the best of a difficult situation when I came home, tackled schoolwork but couldn't always be the husband or father that I wanted to be. If I learned anything at MIT, I learned that my life would lack true meaning without the love that I receive from both Heidi and my daughter Kristin.

Table of Contents:

Chapter 1	Introduction	6
1.1	Hypothesis	7
1.2	Approach	9
Chapter 2	Frequency response characteristics of an air loaded, ring stiffened cylinder in both bulkhead loaded and unloaded configurations	10
2.1	UUV Dummy Payload Section characteristics	11
2.2	Data acquisition methodology	13
2.3	Accelerometer locating criteria	14
2.4	Uncoated shell response behavior	15
2.5	Analysis of bulkhead behavior	21
2.6	Lessons learned; recommendations for lakeside testing program.	23
Chapter 3	Determination of acoustic far field response for a coated cylinder as a function of hydrostatic pressure	24
3.1	Data acquisition methodology	25
3.1.1	Instrument block diagram	26
3.1.2	Hydrophone array considerations	26
3.1.3	Pulse generation and processing	28
3.2	Structural response characteristics of a submerged cylinder	31
3.3	Coating effectiveness as a function of hydrostatic pressure	36
3.3.1	Results	51
3.3.2	Transfer function results	53
Chapter 4	Conclusions	55
References		
Appendix		

List of Figures:

2-1	Internal half section view of UUV cylinder. Accelerometer locations are with respect to the shaker. All dimensions in inches.	11
2-2	Data acquisition block diagram for pre-lake test program.	13
2-3(a)	Shell response in air using 1/6 th octave sampling. No bulkheads loaded.	16
2-3(b)	Shell response in air using 1/6 th octave sampling. Bulkheads loaded.	17
2-4	Total accelerometer power as a function of longitudinal position, measured by summing individual 1/6 th octave sampling point responses.	18
2-5 (a)	Decay sequence for 800 Hz CW pulse without bulkheads loaded. Signal removed at 55 msec.	20
2-5 (b)	Decay sequence for 800 Hz CW pulse with bulkheads loaded. Signal removed at 162 msec.	20
2-6	Instrumentation bulkhead section with radial accelerometer locations. All dimensions in inches.	21
2-7	Bulkhead response as a function of radially mounted accelerometer positions.	22
3-1	Linear, time invariant, space-invariant filter.	26
3-2	Instrumentation block diagram for lake test program	27
3-3	Time series representation for selected channels (Run B45022)	30
3-4	Internal half section view of accelerometer locations with respect to the shaker. Bulkheads not loaded. Accelerometers not to scale.	32
3-5	Channel response characteristics for run B45022	33
3-6 (a)	Accelerometer response (coated and uncoated). 50 feet.	39
3-6 (b)	Accelerometer response (coated and uncoated). 200 feet.	40
3-6 (c)	Accelerometer response (coated and uncoated). 450 feet.	41
3-7 (a)	Hydrophone response (coated and uncoated). 50 feet.	42

3-7 (b)	Hydrophone response (coated and uncoated). 200 feet.	43
3-7 (c)	Hydrophone response (coated and uncoated). 450 feet.	44
3-8 (a)	Coating effectiveness. 50 feet.	45
3-8 (b)	Coating effectiveness. 200 feet.	46
3-8 (c)	Coating effectiveness. 450 feet.	47
3-9 (a)	Bare and Coated transfer functions. 50 feet.	48
3-9 (b)	Bare and Coated transfer functions. 200 feet.	49
3-9 (c)	Bare and Coated transfer functions. 450 feet.	50
3-10	Comparison of hydrophone responses at 50 feet. All hydrophone responses are force and noise corrected.	52

List of Tables:

2-1	UUV Shell and Bulkhead physical characteristics
3-1	Data acquisition summary for runs used during lake test program

Table of Appendices:

Appendix A	MATHCAD™ worksheet . Ring stiffened cylinder coating effectiveness worksheet.
Appendix B	MATLAB™ Data acquisition and Processing Scripts

Chapter 1

Introduction

Coating effectiveness, as measured by the change in a ring stiffened cylinders transfer function, is measured in the acoustic far field for increasing hydrostatic pressures. Coatings can be classified as either reactive or dissipative depending on their intended use. Reactive coatings can be tuned to an expected source frequency in an effort to absorb energy. Dissipative treatments focus on reducing structural vibrations and therefore attenuate waves over a wide band of frequencies. Which type of behavior, absorption for a specific frequency or attenuation for a range of frequencies, is largely determined by the polymers' chemical structure and physical dimensions. In general, polymer coatings produce different results depending upon temperature, frequency, molecular structure of the base polymer, chemical cross-linking systems and filler materials. Of these characteristics, only temperature, frequency and filler materials (indirectly through hydrostatic pressure) can be controlled in a field experiment. This thesis examines one such coating without knowledge of its chemical composition. This 'blind' test measures far field power changes at 50 feet, 200 feet and 450 feet over a pass band of 400 Hz to 10.5 kHz in a constant SVP medium. Since a 10 lbf reactive shaker is mounted to the cylinder's center frame, the approach taken concentrates on understanding the coating as a dissipative treatment.

Point excited finite cylindrical shells have modes that are coupled by radiation when exposed to an ambient fluid. Since a closed form solution is not possible [1], an experimental approach is used. Several formulations for thin shells including Donnell [2] and the Direct Global Matrix [3] method have expanded our knowledge on numerical approaches for simple shells with little or no internal structures. Structural acoustic codes, such as SARA, can be used for

ring stiffened geometries however modeling polymer coatings remains a complexity not present when using an experimental approach.

1.1 Hypothesis

Acoustic waves can be launched by means of a shaker mounted to one of the cylinder's frames. Mounted perpendicular to the flange, the sinusoidal signal produces both a flexural and longitudinal wave on the shell. Though the flexural response is greater (due to direction of the applied force), attenuation of the longitudinal wave, by coating, produce large changes in structural response. As this longitudinal wave propagates into the material, the particles in the region are first forced in the direction of wave propagation and thereafter, for the duration of the wave they are forced back and forth by the oscillations of the wave. This shearing action gives rise to local pressure and density fluctuations. Since the stress is longitudinal, the waves properties are characterized in terms of the corresponding aspect of the Modulus of Elasticity (Young's modulus) of the material. For polymeric materials, shear waves typically travel with very low speeds and are rapidly attenuated; hence the transformation of longitudinal waves into shear waves is greatly desired [4].

For plane waves propagating in an isotropic homogenous medium, the three acoustic properties of importance are: speed of sound, the attenuation coefficient and the specific acoustic impedance of the medium. Since the sound speed is simply the product of the wavelength (λ) and the frequency (f), a decrease in frequency produces a large wavelength. As wavelength increases, less cycles

are attenuated and eventually absorbed as heat. Peak performance typically requires a coating thickness of at least $\lambda/2$ to be effective. Choosing the correct minimum coating thickness is also desirable since at low frequencies the sound power radiated by a rigid cylinder is proportional to the fourth power of the cylinder's diameter [5]. Increased coating thickness also translates to increased structural weight and higher acquisition costs. To increase attenuation of a polymeric material, while minimizing the coating thickness, compliant fillers such as air can be added. The presence of microscopic air bubbles couples the traveling longitudinal wave to the shearing motions at the bubble interface. Since in rubbers the dampening factor for shear motion is orders of magnitude larger than that of longitudinal, the effect of the sound bubble is to dissipate sound energy via the shear dampening factor of the polymer. Acoustic energy will also be incoherently scattered by these bubbles and be subsequently dissipated via multiple scattering. Air also lowers the sound speed and density of the material which affects the acoustic impedance. This change can be offset by the adding a denser filler material such as lead. With increased hydrostatic pressures, coating effectiveness should decrease due to collapse of the microscopic air bubble which thereby reduce attenuation due to scattering. Expected coating behaviors can be summarizes as:

1. Coating reduces far field response under constant forcing.
2. Coating reduces transfer function.
3. Coating effectiveness decreases with depth due to collapse of microscopic air bubble fillers.

4. Coating effectiveness decreases below some cutoff frequency.

1.2 Approach

To measure the far field response change due to the application of a dissipative coating requires knowledge of the acoustic medium. Since the propagation of small-amplitude acoustic signals in an unbounded or bounded fluid medium can be described by the linear wave equation, we can treat such as a linear filter. For a linear time-invariant (LTI) system, Fourier Transforms provide a framework for solving problems. If the filter (coating) does not change with time then the filter response can be expressed simply as the quotient of the output to the input. Accuracy of results would then depend on how well the source and receiver were instrumented.

Since instrumentation resources are limited to 16 channels, a carefully designed test program is essential. Accelerometer response is a strong function of its location, longitudinal or radially measured, with respect to the shaker source. Finite, ring stiffened cylinders also provide multiple means of reflection of the input signal along the cylinder's shell structure. Hydrophone arrangements need to consider spacial coverage. For these reasons, a pre-lakeside test program measuring the cylinder's frequency response to a sinusoidal input was conducted for a 3 octave band (400 Hz to 4032 Hz). Lessons applied prior to the lakeside test program include instrumentation location, pulse type determination, frequency band coverage and a coating coverage plan for both shell and bulkheads.

Chapter 2

Frequency response characteristics of an air loaded, ring stiffened cylinder in both bulkhead loaded and unloaded configurations.

The frequency response for an uncoated ring stiffened cylinder for two different structural configurations is investigated. These two structural configurations differ by the addition of twin bulkheads; used to make the cylinder watertight during the lake testing program. Characterized by a superposition of radial and longitudinal modes, the cylinder's measured frequency response will vary as a function of accelerometer placement. For lake testing, a maximum of 16 instrumentation channels are allotted. With these channels, accelerometer input power, hydrophone far field response and leak detection monitoring is accomplished. Given these limited resources, a pre-lake testing program establishes not only the number, but the optimal accelerometer placement, required to capture an approximation of the cylinder's behavior. True behavior can only be measured in the far field, however an accurate input is needed for the subsequent linear filter approach which is used for calculating transfer functions.

In addition to waterproofing, bulkheads tend to increase the objects noise level due to the coupling between the dynamics of the cylinder shell, bulkheads themselves and the inner cavity. The natural modes of the separate components frequently "force" their response on each other leading to conditions where the shell modes, end modes, and couple modes (shell and end) force a large acoustic response in the interior (and exterior) even at frequencies where no natural interior cavity mode exists [7]. Cheng observed that at low frequencies ($< \sim 400$ Hz), the ends tend to couple more efficiently to the interior than do the shell modes and that shell / end coupling tends to be weak [8]. This would imply that higher frequencies, as would be seen in this experiment, will produce large acoustic energies due to coupling. Modes can be uncoupled

through the use of coating treatments placed on the bulkhead sections. Examination of the bulkhead responses also provide information on how much energy is radiated through the end caps as compared to the shell structure.

2.1 UUV Dummy Payload Section characteristics

The ring stiffened cylinder used for this experiment was obtained from the Advanced Research Projects Administration (ARPA) Unmanned Underwater Vehicle (UUV) program. The dummy payload section is a titanium shell with ring stiffened 'T' frames. With a design depth of 1000 feet, stiffening is required to prevent shell buckling. Titanium, when compared to conventional steel ($\rho g = 487 \frac{\text{lb}_f}{\text{ft}^3}$), provides a higher yield strength and superior anti-corrosion behavior for a density that is just 56 percent of the latter. Added longitudinal strength is provided on the UUV's Instrument Pass side through the use of equally spaced stringers. These stringer plates are perpendicular to the bulkhead mating ring and are spaced at 4 inch intervals between the first inside T-frame and the bulkhead lip. Figure 2-1 shows a half section view of the cylinder, along with the internal accelerometer arrangement.

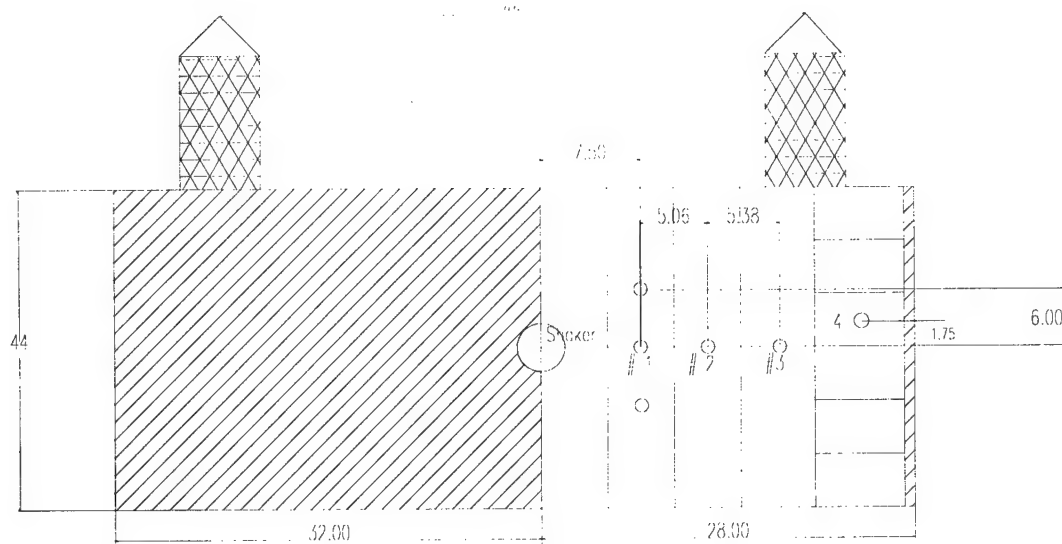


Figure 2-1: Internal half section view of UUV cylinder. Accelerometer locations are with respect to the shaker. All dimensions in inches.

Each tested configuration includes a 4 point, steel fabricated sound isolated platform. This platform is installed should additional in-hull instrumentation packages become necessary during the lake testing program. For each test run, the cylinder is hoisted above its cradle using twin six inch wide nylon straps. These straps allow motion in each of three principle degrees of freedom (axial, radial and tangential) thereby approximating a free-free boundary condition. Table 2-1 provides a summary of shell, framing and bulkhead dimensions along with their physical properties. Throughout this paper, English Customary units are used; MKS units are provided, for reference , as appropriate.

Table 2-1: UUV Shell and Bulkhead physical characteristics

UUV Cylinder Characteristics	
Shell and Frame Material	Titanium 6A1-4V
Young's Modulus, E	16.5 Msi (113.7 Gpa)
Density	$276 \frac{lb}{ft^3}$ ($4430 \frac{Kg}{m^3}$)
Poisson's Ratio	0.3
Longitudinal Length	60 inches (1.52 m)
Diameter	44 inches (1.12 m)
Shell Thickness	0.25 inches (6.4 mm)
Frames (Radial)	9
Frame spacing	5 inches (127 mm)
Frame Dimensions	
Height Web (H_W)	0.19 inch (4.8 mm)
Thickness Web (T_W)	1.88 inch (47.6 mm)
Height Flange (H_F)	1.50 inch (38.1 mm)
Thickness Flange (T_F)	0.19 inch (4.8 mm)
Fillet size	0.25 inch (6.4 mm)
UUV Bulkhead Characteristics	
Bulkhead Material	Aluminum 6061-T6
Young's Modulus, E	10.5 Msi (72.4 GPa)
Density	$169 \frac{lb}{ft^3}$ ($2700 \frac{Kg}{m^3}$)
Poisson's Ratio	0.3
Diameter	44 inch (1.12 m)
Thickness (less cruciform)	2 inch (50.8 mm)
Stiffener arrangement	Cruciform; 2 inch square bar

2.2 Data acquisition methodology

Evaluation of the cylinder's response spectrum uses the instrumentation setup provided in Figure 2-2. With this arrangement, a 2 channel spectrum analyzer (HP-3563A) generates a waveform signal that is converted to a mechanical impulse via a 10 lbf electromagnetic reaction type shaker (Wilcoxon Research Model F7/F4 Shaker). An amplifier and matching network provides a smooth transition above the F4 shaker's upper limit of 7.5 kHz [9]. For the pre-lake test program, shaker use is limited to the range designed for the F4. A three octave test program provides ample frequency coverage to determine structural behavior in both bulkhead loaded and unloaded configurations. This range was subsequently expanded to 4032 Hz in order to capture elevated responses at 3200 Hz.

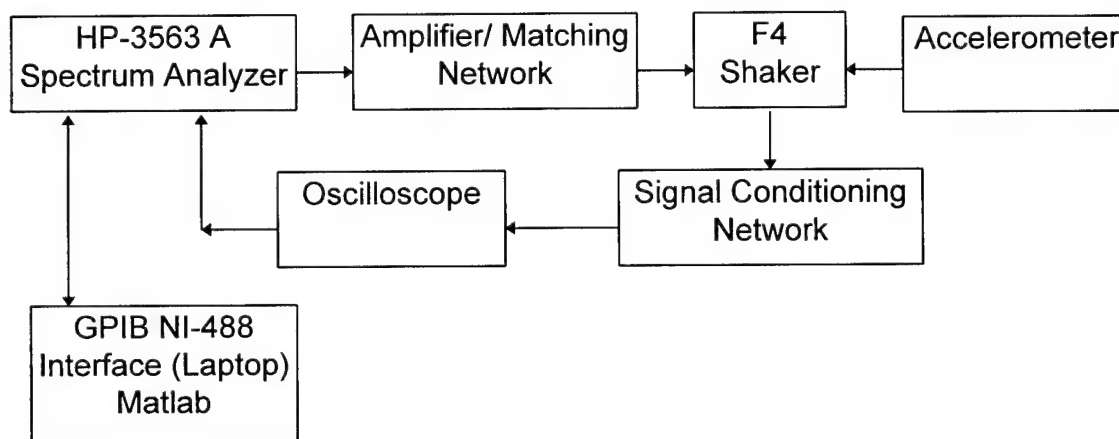


Figure 2-2: Data acquisition block diagram for pre-lake test program

Time domain behavior is translated into the frequency domain by using the spectrum analyzers Fast Fourier Transform (FFT) function. Sample rate for all measurements was 25 kHz, well above the aliasing threshold. Digitized data is then interfaced to a laptop using a PCMCIA NI-488 GPIB board. ASCII data is text processed to remove header information, then ported to MATLAB™ for display and analysis purposes.

2.3 Accelerometer locating criteria

Accelerometers measure the frequency response of a vibrating structure. For this experiment, three Vibrametric Model 2002A accelerometers with a rated sensitivity of 10 mV /g are used and relocated as required. These piezo-electric accelerometers have a calibrated linear response up to 10 kHz with minor degradation between this upper limit and 20 kHz [10]. Accelerometer clipping occurs for signals in excess of 250 g's . For the shell evaluation without bulkheads, the HP-3563A source voltage is set to 0.8 volts. This produced a maximum response that was less than 25 g's. To provide a more mid range response, the gain was increased to 4 volts for the bulkhead loaded configuration runs. Increasing gain is acceptable since the subsequent increase in signal is linear. With an understanding of accelerometer operating characteristics, the placements were based on the following hypothesis, namely:

1. Response decays along a longitudinal axis. Four accelerometer positions are chosen between the shaker and the instrumentation bulkhead mating ring. These positions, as shown in Figure 2-1, are at the midpoint of each frame bay with the exception of one accelerometer located just off the longitudinal axis in an adjacent stringer bay. Since the shaker generates both a flexural and longitudinal wave, it is expected that the longitudinal wave will be scattered by the frames due to a change in impedance and thereby show a reduced response as a function of position.
2. Radial response inside a frame bay is symmetric with respect to the longitudinal axis. Symmetry dictates that the responses of two accelerometers equally spaced from opposite sides of a longitudinal line should have similar responses. Small deviations are expected as accelerometer placements near the sound isolated platform due to dampening from the isolation mounts.

3. Outside shell structure response matches inside shell responses.

Accelerometer pairs are located on either side of the shell along a radial line. A linear filter treatment requires knowledge of the input's power level to the coating/acoustic medium (fresh water). Power levels recorded at the inside shell should match power levels on the radial line except for small variations due to longitudinal waves along the shell.

4. Bulkhead response is significantly less than shell response. The bulkheads are located at either end of the longitudinal axis. With attenuation due to frames, bulkhead response should be a fraction of shell response. Five accelerometers are located on a 45 degree radial line situated between two cruciform stiffeners.

To test these assumptions, a 1/6th octave sampling grid is established. This sample grid provides 6 sample points per octave and therefore provides 21 points between 400 Hz and 4032 Hz. Increased sample frequency discounts the effects of nodes and elevated (near resonant) responses. CW pulses are used to provide superior signal strength. Random noise sources were evaluated as being unsuitable due to the lengthy processing time needed for frequency resolution.

2.4 *Uncoated shell response behavior*

The frequency response for the ring stiffened cylinder, without bulkheads loaded, is presented in Figure 2-3(a). CW pulses, using an HP-3563A source voltage of 0.8 volts, were taken for a pass band of 400 Hz to 4032 Hz. Smoothing was done using a polynomial trendline fit. Smoothing of individual octave sample points provides a representation of the spectrum, however it does not adequately define the shape of resonant and nodal points away from the sample grid.

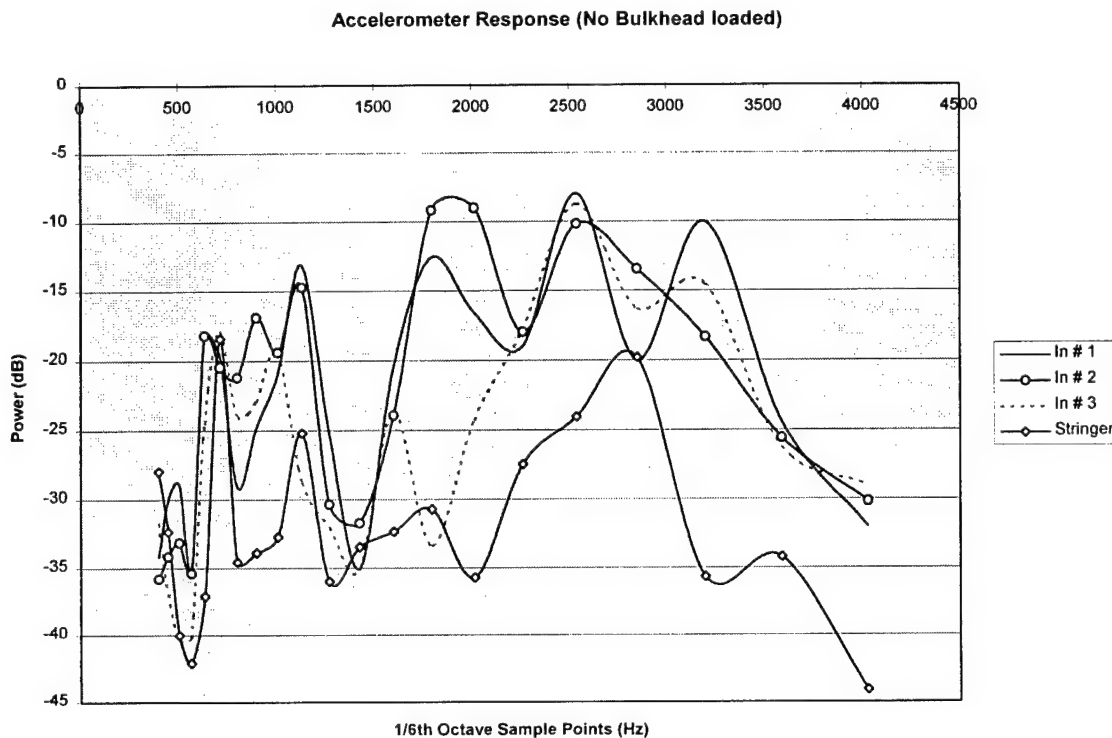


Figure 2-3 (a) : Shell response in air using 1/6 th octave sampling. No bulkhead loaded

Repeatability of results required careful monitoring of strap positions during lifting operations and the use of digital function generators instead of analog units. Analog function generators, such as the BK Precision Model 3011B produced large, not repeatable, ranges of accelerometer responses. The function generator uses an analog tuner to generate its waveform with an LED readout of ± 1 Hz for values less than 1 kHz and then ± 10 Hz for values between 1 kHz and 20 kHz. Since large variations are noted for even a 2 Hz change in frequency, use of analog units was deemed unacceptable. Figure 2-3 (b) provides a comparison of the frequency response for the shell with the bulkheads being loaded.

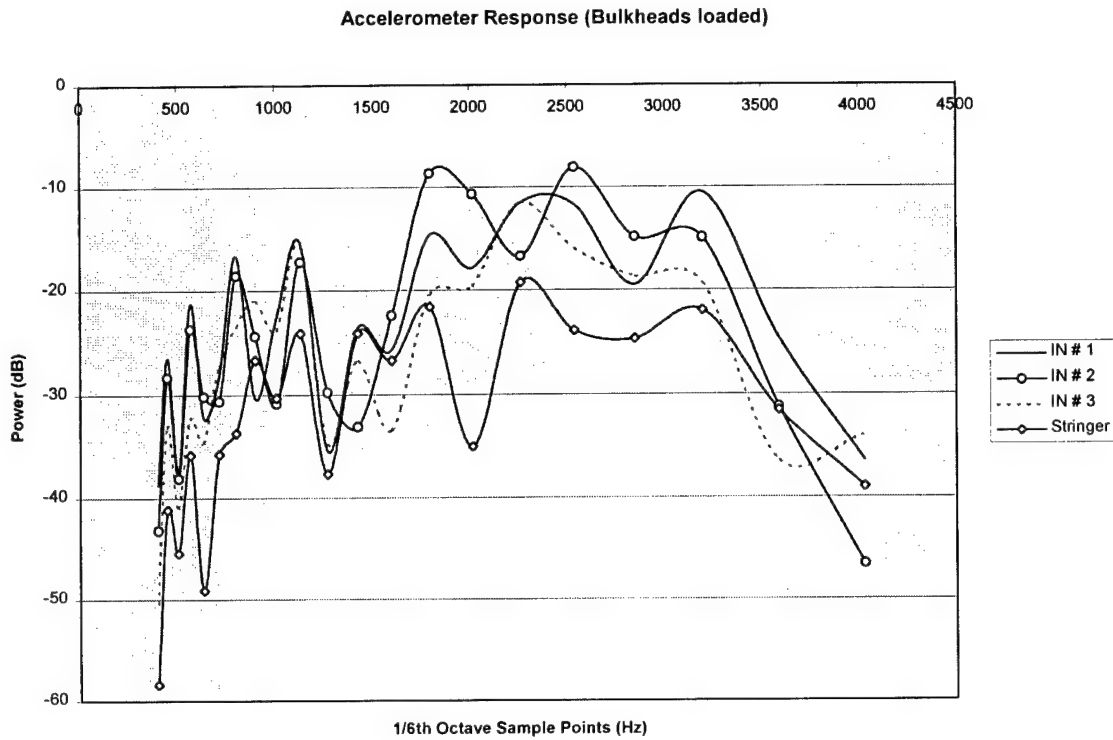


Figure 2-3 (b): Shell response in air using 1/6 th octave sampling. Bulkheads loaded.

In order to compare these two configurations, the *band contribution*, $(p^2_b)_{av}$, which is a measure of the power level for a specific band of frequencies is calculated. For a continuous frequency band, the mean square power is just the spectral density function over the frequency band of interest, or:

$$(p^2_b)_{av} = \int_{f_1}^{f_2} p_f^2(f) df \quad (2.1)$$

Since discrete frequencies are being measured, we use the discrete form of Eqn 2.1, which is known as the *weighted mean square power* $(p^2)_{av,W}$:

$$(p^2)_{av,W} \approx \sum_b W(f_{0,b}) (p^2_b)_{av} \quad (2.2)$$

The weighting factor, $W(f)$, is frequency-dependent and varies depending on the relative response functions that are used [11]. For this experiment, a flat response is chosen, defining a unity weighting factor. Using this form, we remove some bias that would be introduced from curve fitting and instead take only the power levels for each of the 1/6th octave sampling points. Figure 2-4 provides a representation of total band power (dB) as a function of longitudinal position measured from the shaker for both structural configurations.

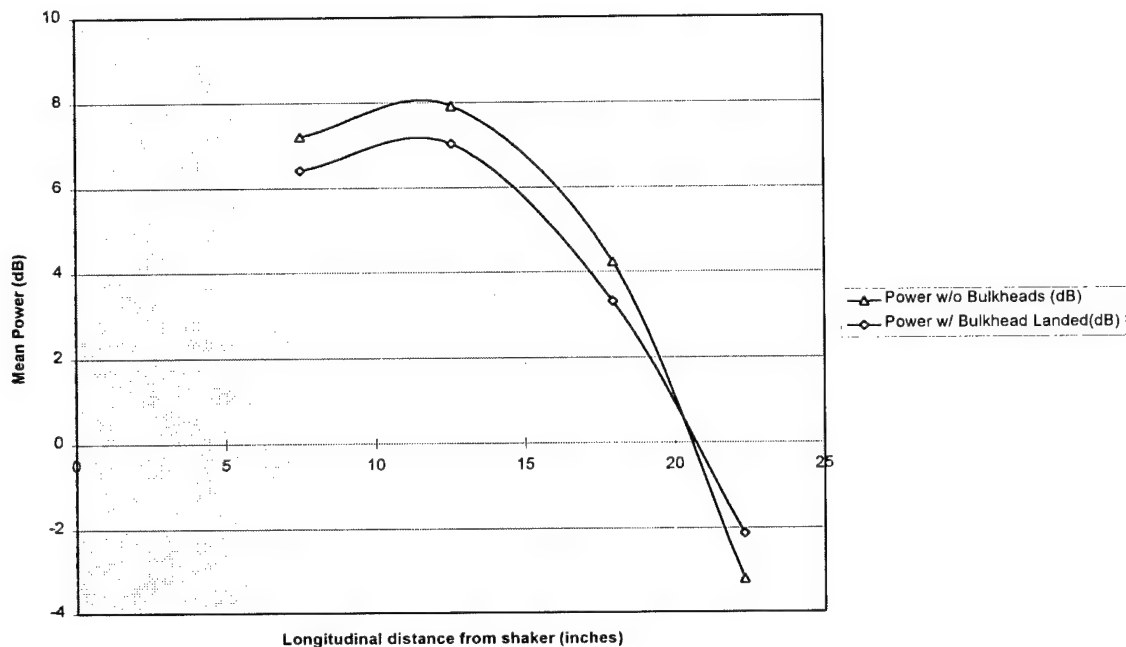


Figure 2-4: Total accelerometer power as a function of longitudinal position as measured by summing individual 1/6 th octave sampling point responses

From this graphic, we note that accelerometer power is affected by both the stiffener frames and by the bulkhead. Stiffeners act as an impedance boundary to the longitudinal wave. Depending on the frequency, the frames scattering behavior provides the longitudinal wave a window to be either passed or stopped. Bulkhead placement is similar to frames in that the bulkheads provide a scattering mechanism for the waves. To examine this behavior, decay rates are

measured for one frequency (800 Hz). This single frequency was chosen prior to the experimenter's knowledge of stop and passband behaviors. For this reason, no direct conclusions can be reached about decay rates except for behavior at this single frequency.

To calculate decay rates, a CW pulse was generated for both the bulkhead loaded and unloaded configurations. Measurements were taken, in both cases, at accelerometer # 3 which is 17.9 inches from the shaker center. The time series for the bulkhead unloaded and loaded sequences are presented in Figures 2-5 (a) and(b) respectively. In the loaded configuration, a least squares analysis was conducted using the maximum wave amplitude for the wave packet. The least square analysis provides an upper bound of decay rate and was calculated as $0.067 \text{ dB} / \mu \text{ sec}$. As a comparison, this number was compared to a decay rate calculated by Park [12] who examined the structural behavior of a nickel shell with internal frames subject to a broadband signal. In the Park experiment, a decay rate of $0.051 \text{ dB} / \mu \text{ sec}$ is calculated. The cylinder, used by Park, had a higher length to diameter ratio ($L/D = 6.65$) compared to the UUV section ($L / D = 1.36$) used in the experiment. In Park's cylinder, four frames were placed in a non-uniform bay interval. This UUV section has 10 uniformly spaced frames. With a smaller L/D , tighter integration of frames a higher decay rate would be expected for the UUV section.

Calculations for the unloaded condition, also using a least squares analysis, produced a decay rate of $0.071 \text{ dB} / \mu \text{ sec}$. No conclusions can be made for this frequency since both conditions produce effectively the same results. Further study evaluating decay rates as a function of frequency, may provide greater insight to signal decay with respect to bulkhead and frame geometry.

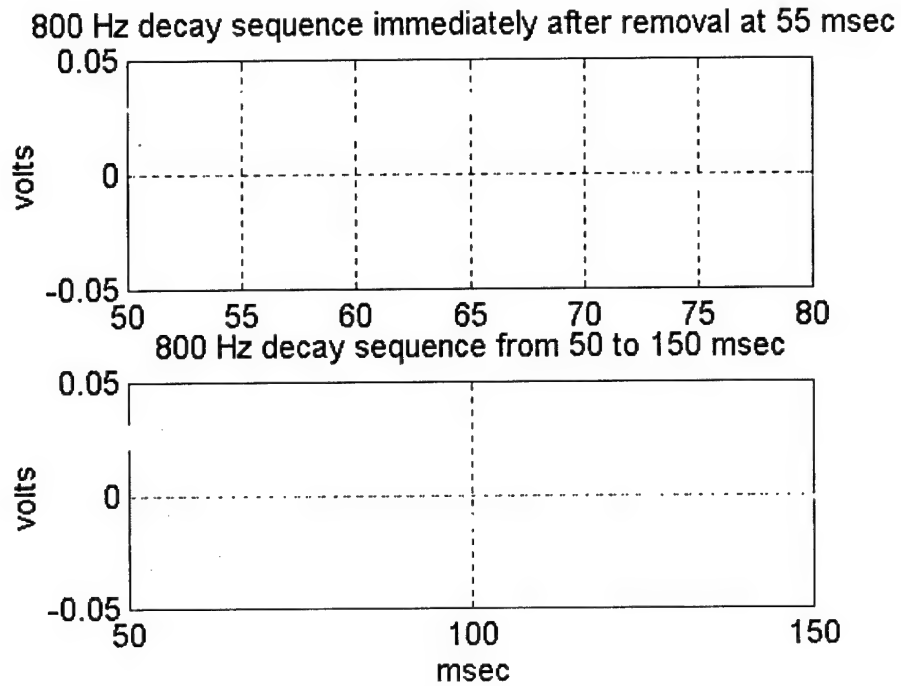


Figure 2-5 (a): Decay sequence for 800 Hz CW pulse without bulkhead loaded. Signal removed at 55 msec.

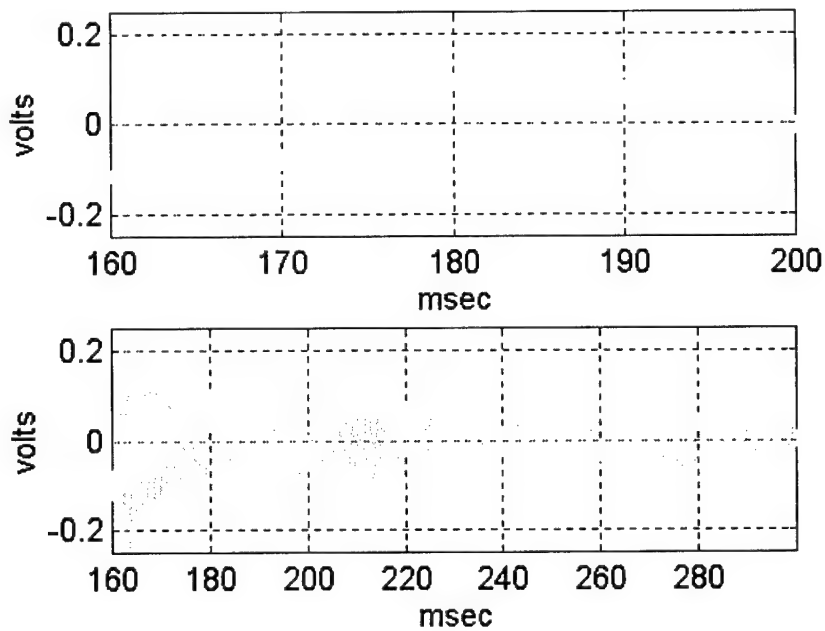


Figure 2-5 (b): Decay sequence for 800 Hz CW pulse with bulkhead loaded. Signal removed at 162 msec.

2.5 Analysis of bulkhead behavior

Bulkheads are used to make the UUV section a watertight vessel. For the experiment, two similar anodized aluminum bulkheads are used. Figure 2-6 shows the instrument pass through bulkhead.

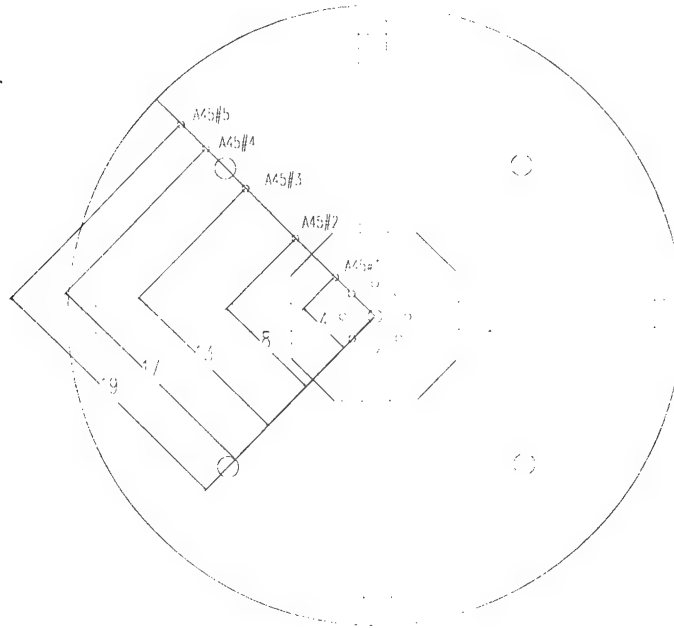


Figure 2-6: Instrumentation bulkhead section with radial accelerometer locations. All dimensions are in inches.

This bulkhead provides the means for interfacing the cylinder's internal equipment stack with the control and measuring instrumentation. Interfacing is accomplished using BRANTNER™ type connectors which are podded prior to the lakeside test program. To evaluate the radiative power from this end enclosure, the response is measured by five radially mounted accelerometers. These accelerometers are placed near discontinuities such as BRANTNER™ interface connections and near the cruciform stiffeners. Individual accelerometer responses are recorded using a 1/6th Octave grid for a band of 566 Hz to 4032 Hz using a source voltage of 4 Volts. Sample responses below this threshold

were indistinguishable (< 5 mV) from background noise. Results are presented in Fig 2-7.

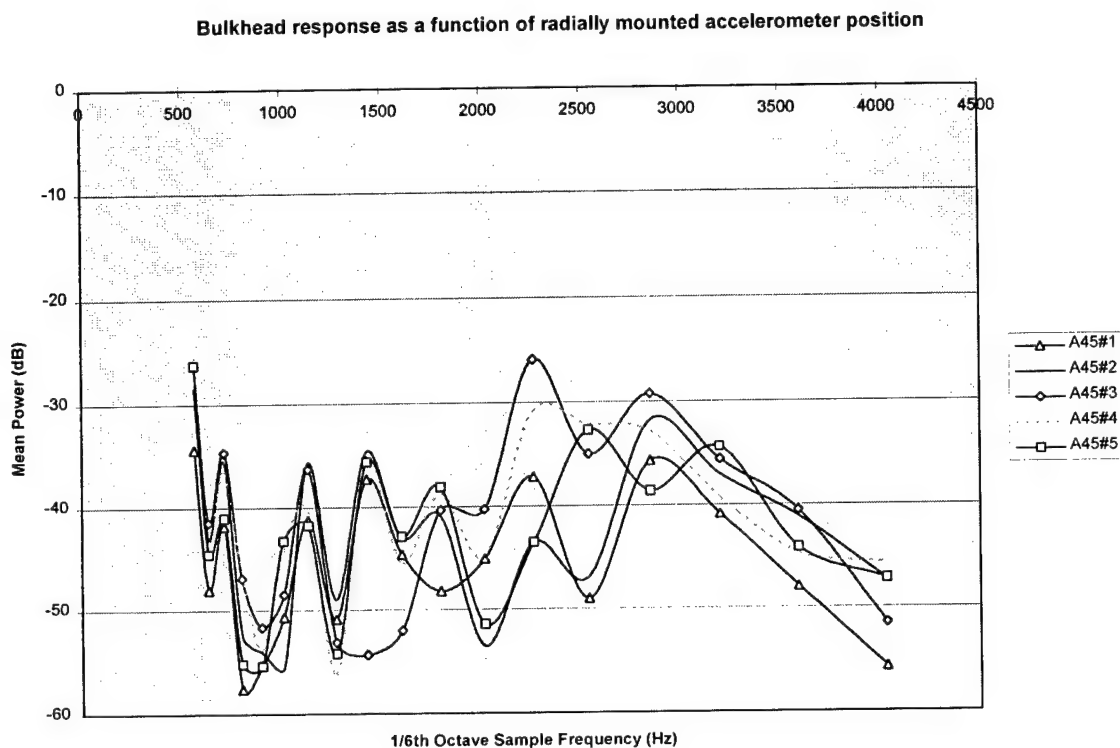


Figure 2-7: Bulkhead response as a function of radially mounted accelerometer positions

Power levels recorded from these runs show that the response is comparable to those received from the stringer accelerometer runs and represents a value that is 5 to 10 percent of the values recorded for accelerometer # 1. Since bulkheads are significant radiators, decoupling will be used.

2.6 Lessons learned; recommendations for lakeside test program

The purpose of the pre-lake test program was to gain familiarity with the structural response of the cylinder, evaluate accelerometer placements and to gain familiarity with data acquisition techniques. From this exercise, the following lessons were provided for use in the lake testing program.

1. Frequency Bin sampling will be used instead of discrete sample points. The repeatability of 1/6th octave sample points was a function of boundary conditions, bulkhead loading conditions, instrumentation accuracy and accelerometer placement. Since specific frequency determination of coating effectiveness is not required, a frequency bin approach should be pursued. With a pass band of 10.1 kHz, averaging over power levels for units of 500 Hz will remove sensitivity to shifts in resonance's and nodes seen in the pre-lake test program.
2. Source signal should be Linear Frequency Modulation (LFM). LFM offers the signal strength of CW pulses and the sweep coverage of random or white noise signals.
3. Apply decoupling treatment to bulkheads. Decoupling treatments will reduce far field radiated power from the bulkhead face and will act to decouple modes between the shell and the bulkhead.
4. Accelerometers need to only be placed on the inside shell. Accelerometer measurements conducted on the outside shell are nearly identical to those recorded from inside units. Inside placement is consistent with the planned linear filter approach. With 16 available channels, nine accelerometers will be placed on the inside shell to accurately measure the cylinder's response.

Chapter 3

Determination of acoustic far field response for a coated cylinder as a function of hydrostatic pressure.

Coating effectiveness, as measured by the change in a ring stiffened cylinders transfer function, is measured in the acoustic far field for increasing hydrostatic pressures. As described in Chapter 1, polymer coatings produce different results depending upon temperature, frequency, molecular structure of the base polymer, chemical cross-linking systems and filler materials. Without knowledge of the polymer's composition, effectiveness can still be gauged by varying the input frequency and indirectly the filler composition through increasing hydrostatic pressures. Hydrostatic pressure tends to collapse the microscopic air bubbles used to convert longitudinal waves to shearing waves. As the bubble diameter is reduced, the coating effectiveness should also decrease.

To test this hypothesis, a deep water facility is used. The Acoustic Research Detachment, Lake Pend Oreille, Idaho was the site of the deep water test program. Testing was conducted in conjunction with Science Applications International Corporation (SAIC) from 3 March and 12 March 1997. Lake Pend Oreille is well suited for this task since the Yellow Barge Test Facility sounding exceeds 1000 feet with a nearly constant year round (depths > 25 feet) sound velocity profile. Surface noise is seasonal; based on lake activities such as boating and wind. During the March test period, boating was minimal however wind conditions forced early morning testing due to surface noise and increased motion of the barge. Reducing ambient noise improves SNR.

Given these deep water capabilities, the experiment is conducted for a frequency pass band of 400 Hz to 10.5 kHz. This increased bandwidth, explained in the instrumentation section, provides sufficient coverage to gauge coating effectiveness as a function of wavelength. To measure the response as a function of hydrostatic pressure, the cylinder is tested at three different operating

depths, namely 50 feet , 200 feet and 450 feet. These depths were chosen to evaluate the effectiveness near the surface (50 feet) , at an intermediate depth (200 feet) and near the maximum operating depth (450 feet). A finite element analysis [12] calculated that the aluminum bulkheads, utilizing a safety factor of 1.25, would yield at 511 feet. Multiple test runs were conducted to account for uncertainty in the relative position of the cylinder's beam with respect to the hydrophone array. Since the test is conducted in the far field, some inaccuracies can be tolerated. Use of a line array mitigate uncertainties due to relative position.

Relative motion of the cylinder can be expected due to deep lake currents or the afro mentioned translation of the barge due to wind. Since the enclosed cylinder is positively buoyant (3514 lbf), lead ballast is required for submergence. With a dead weight of 1500 lbf, 2800 lbf of ballast provides sufficient negative buoyancy to submerge the cylinder and to keep rotational movements to a minimum. Calculations to support cylinder testing are presented in Appendix A.

3.1 Data acquisition methodology

For acoustic signals, fresh water be treated as an inviscid fluid. Since the propagation of small-amplitude acoustic signals in an unbounded or bounded fluid medium can be described by the linear wave equation, we can treat such as a linear filter. For a linear time-invariant (LTI) system, Fourier Transforms provide a framework for solving problems. If the filter (cylinder structure, coating and fresh water) does not change with time then the filter response can be expressed simply as the quotient of the output to the input. This approximation is valid since testing is conducted for a fixed hydrostatic pressure in both a coated and uncoated configuration. The LTI space-invariant filter used in this experiment is shown in Figure 3-1. The filter network can be characterized by its time-invariant, space-invariant impulse response $h(t, \mathbf{r}; t-t_0, \mathbf{r}-\mathbf{r}_0)$ which describes the response of

the filter at time t and spacial location $\mathbf{r} = (x, y, z)$ due to the application of a unit-amplitude impulse t_0 and spacial location $\mathbf{r}_0 = (x_0, y_0, z_0)$.

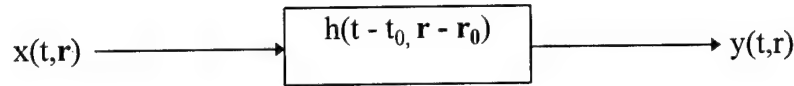


Figure 3-1: Linear, time invariant, space-invariant filter

3.1.1. Instrumentation block diagram

Using this linear filter approach, the objective becomes how to accurately record both the filter input and output signal using the minimum number of resources. For this experiment, the number of available data channels is limited to 16. These channels are responsible for recording the filter input (accelerometers), the filter output (hydrophones), providing a leak detection monitoring function and recording the input force to the cylindrical structure. The input force (Channel 10) is needed since we are using the Wilcoxon Research Model F7/F4 Dual Shaker System with a PA7C Power Amplifier for a changing hydrostatic loading condition. As the frequency band is swept, both shakers can be driven simultaneously. As the force output of the low frequency electromagnetic generator drops off, the force output from the piezoelectric (F7) generator increases for a smooth crossover between vibration generators for automatic frequency sweeps. The useable frequency ranges are: F4 (10 to 7500 Hz) and F7 (500 to 20 kHz). The instrumentation block diagram used for this experiment is shown in Figure 3-2.

3.1.2 Hydrophone array considerations

A five element segmented vertical line array is used to measure the far field response from the cylinder. Far field responses permit using the data without making phase corrections due to wave front curvature. Junger and Feit [1]

define the far field to be the range required to achieve the following criteria, namely:

1. Pressure follows a spherical spreading loss; amplitude decaying as R^{-1} .
2. Angular dependence of the pressure amplitude does not vary with R .
3. Specific acoustic impedance equals characteristic, plane wave impedance.

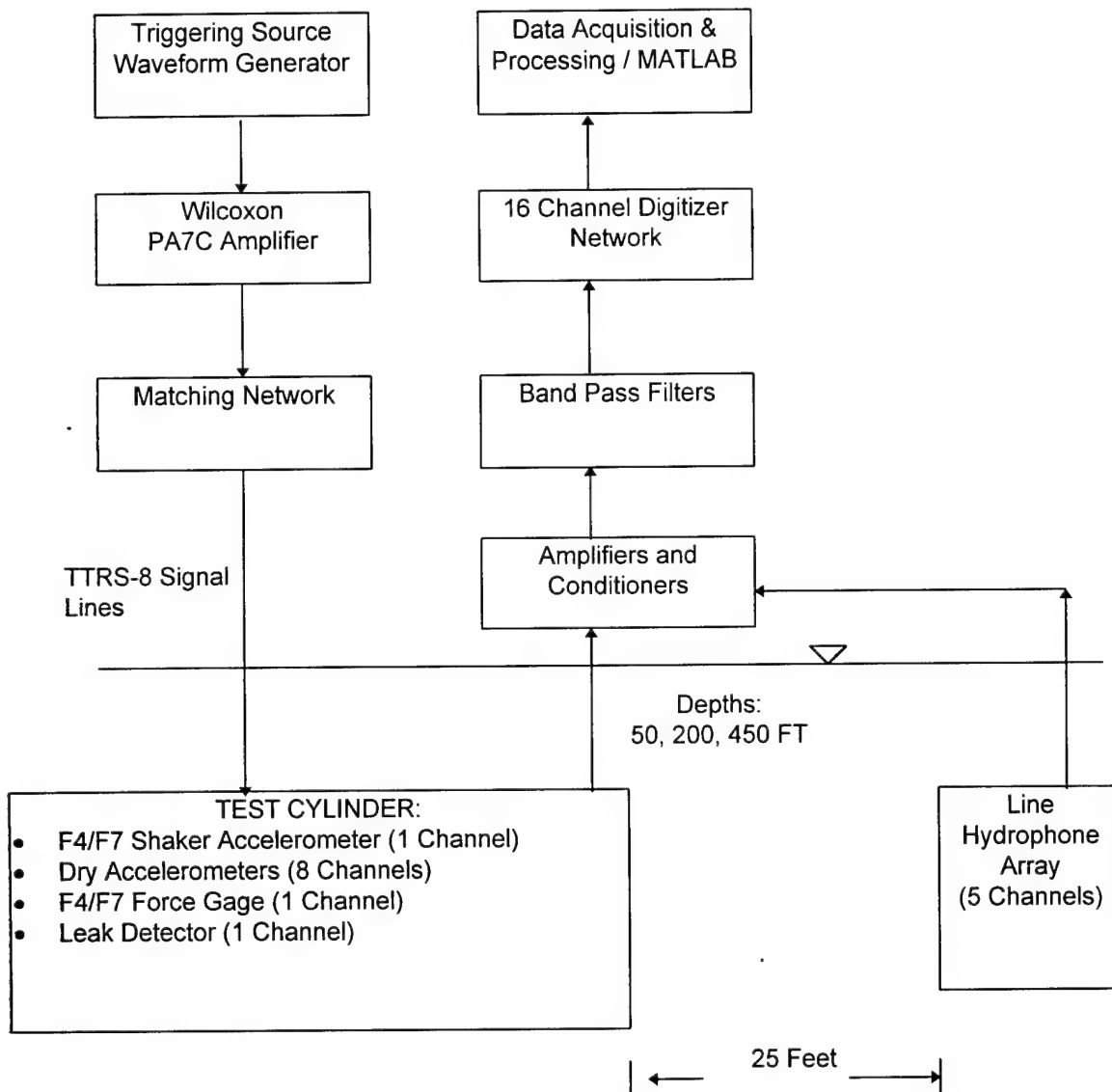


Figure 3-2: Instrumentation block diagram for lake test program

Since 1 and 2 define the Fraunhofer zone, these conditions are satisfied if the source amplitude is small in terms of wavelength. The smallest wavelength occurs at $f = 10.5$ kHz ($\lambda = 20$ inches) therefore the first two criteria are easily met. The third far field criterion effectively adds a range restriction that :

$$k(R - R_o) \gg 1 \quad (3-1)$$

This criteria ensures that the radius of curvature of the wavefront is large in terms of wavelength. A choice of $k(R - R_o) = 10$ is achieved for distances greater than 21 feet. A calculated quadratic phase factor [13] value of 0.787 also confirms far field conditions. Choosing a reasonable far field location is dictated by environmental concerns since increased noise reduces SNR.

The proposed line array spacing also addresses spatial coverage. Since the volume aperture is cylindrical, a vertical line array should produce similar results for each hydrophone. Since beamforming is not being accomplished, a 6 foot separation between hydrophone elements is chosen to provide a 51 degree arc of coverage with respect to the cylinder's beam.

3.1.3 Pulse generation and processing

For each data acquisition run, a waveform signal is generated and the responses captured using a 16 channel digitizer. Each run, consisted of a 1.317 second time window which can be further decomposed into three different time sequences. These sequences consist of the time for filter settling, time for pulse generation and propagation time from the cylinder to the farthest hydrophones. Understanding this time sequence is crucial to matching response with frequency.

Employing a lesson learned from the pre-lake test program, the pulse choice becomes Linear Frequency Modulated (LFM). LFM pulses, also known as swept

CW, provide a means of ramping a CW signal through the passband of interest. LFM signals are extensively used in the design of sonar systems due to its superior Doppler and range resolution features. To represent an LFM signal, a complex envelope is needed. Complex envelopes [13] provide a simple representation of amplitude and angle modulated carriers which are useful in analysis. The rectangular - envelope LFM pulse can be generated by the following expression, namely:

$$x(t) = a(t) \exp(+jD_p t^2) \quad (3.2)$$

$a(t)$ represents the amplitude modulating signal, D_p represents the phase deviation constant and t is time. The deviation constant is defined in terms of the pass band frequency and the elapsed signal time or

$$D_p = \frac{\pi(f_c - f_i)}{(t_c - t_i)} \quad (3.3)$$

Since 16 channel data acquisition is being used with a 25 kHz sample frequency, a 1.317 sec sample window is calculated. Propagation time from the shell to the farthest hydrophone using the speed of sound for fresh water ($c = 1460$ m/sec) yields 0.006 seconds. Filter settling time, for the yellow barge filters, was provided as 0.3276 seconds. The difference between the latter two times and the sample window yields the pulse duration. Providing for a slight uncertainty in pulse propagation time (0.01 sec) yields a pulse duration of 0.973 seconds.

Sixteen channels provide 32767 positive data points per channel. An example of the responses, as seen by 4 different channels is provided as figure 3-3. These time series were then converted to the frequency domain using an FFT approach. Unlike the pre-lake test program which used 1/6th octave sampling, we are now free to explore different methods of response representation as a

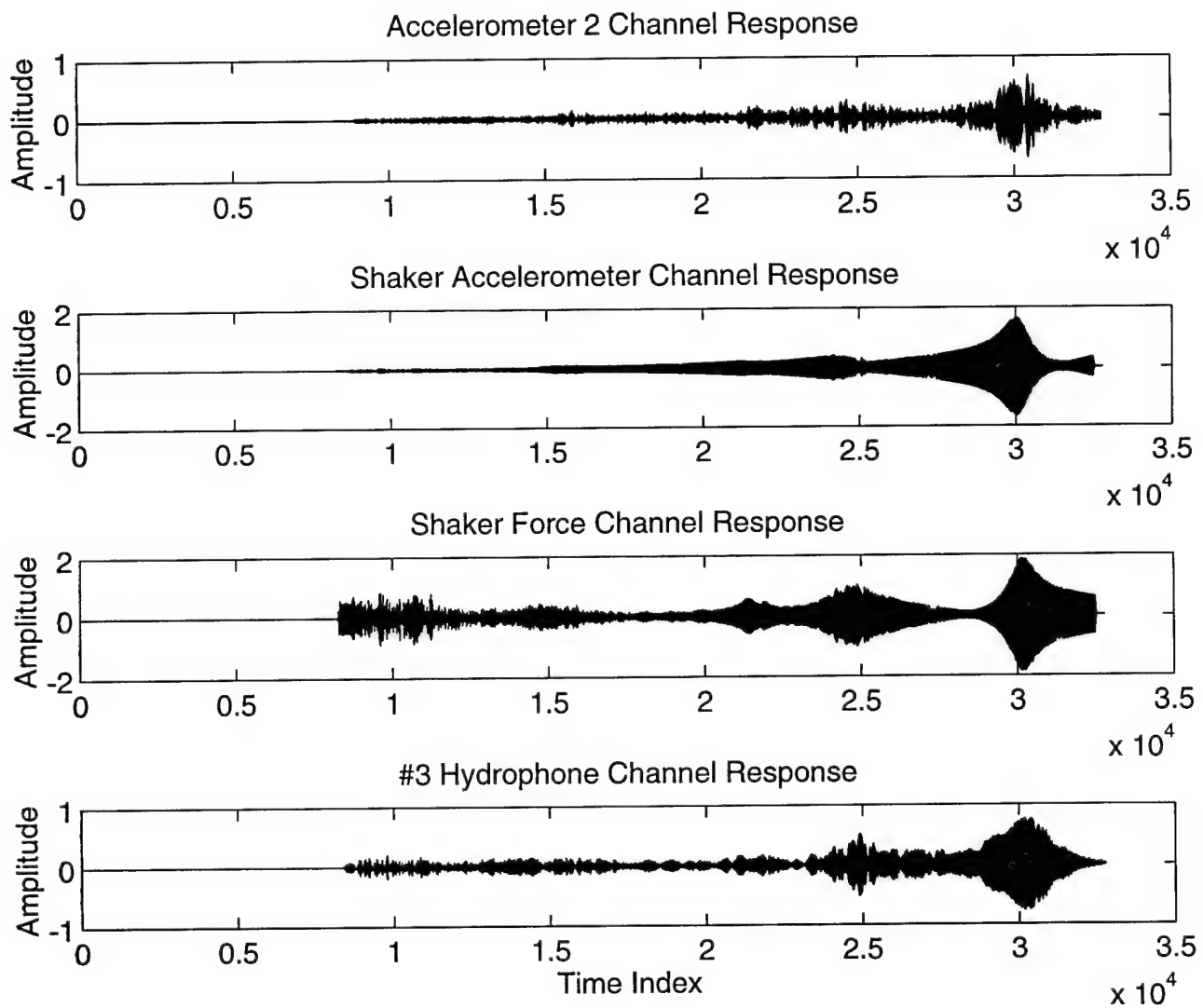


Figure 3-3: Time series responses for four selected channels

function of frequency. Since an LFM pulse covers the given pass band and specific frequency responses are not needed, a frequency bin approach can be used. Frequency bins offer the ability to average over a fixed band of frequencies thereby removing biases due to nodes or resonant points. Slight changes in boundary condition, such as depth changes or rigging, are less volatile when compared to results received using 1/6th octave sampling.

Bins are sized at 100 data points each. Since 15 channels of processed data are used (recall one channel is used for leak detection only), 22 bins are created for each channel with a frequency bandwidth of 459.1 Hz. Each bin's average power level is provided at the band's center frequency which range from 629 Hz to 9871 Hz. Data processing is accomplished using signal decomposition routines such as PLOTRES. Appendix B provides a list of key MATLAB scripts.

3.2 *Structural response characteristics of a submerged cylinder*

With the waveform selected, the 9 accelerometers (including the shaker accelerometer) were located in a manner similar to the pre-lake test program. The accelerometer layout, shown in Figure 3-4, adds two additional accelerometer channels longitudinally (channels 7 and 8) to improve averaging and for further evaluation of accelerometer response as a function of longitudinal position.

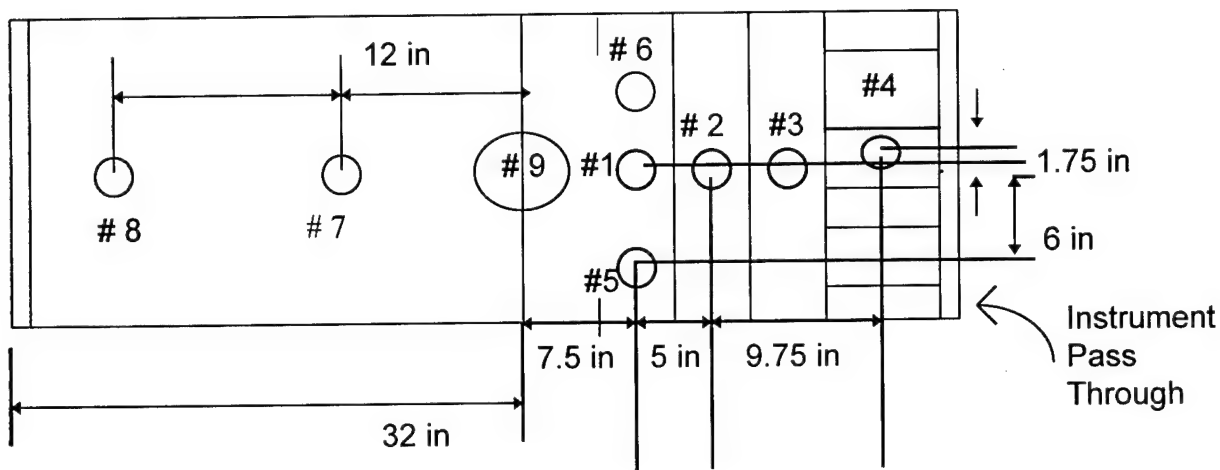


Figure 3-4: Internal half section view of accelerometer locations with respect to the shaker. Bulkheads not loaded. Accelerometers not shown to scale.

The structural response characteristics, as a function of instrument channel, were then compared simultaneously to evaluate responses between the channels. The channel assignments used are as follows: 9 accelerometer channels (1-9), one force channel (10) and the five hydrophone channels (10-15). The remaining channel (16) is reserved for leak detection purposes. Figure 3-5 provides a snapshot of one bare hull configured run taken at 450 feet. As expected, the accelerometer channels all have different responses characteristics indicative of the different modes that being sensed at any particular accelerometer location. From the pre-lake testing program, it was shown that the responses are highest for locations within 12 inches (2 frame bays) of the shaker. For this reason, the majority of the accelerometers are located within 12.5 inches of the shaker. The maximum response is recorded for the shaker accelerometer channel (9), with the force channel normalized to unity. As expected, the response characteristics for accelerometer channels 2 and 7 are similar since they are located on either side of the shaker at a distance of 12 inches. The minimum high frequency response corresponds to channel 8 (stringers) most probably due to the extra structural impedance of the longitudinal plates.

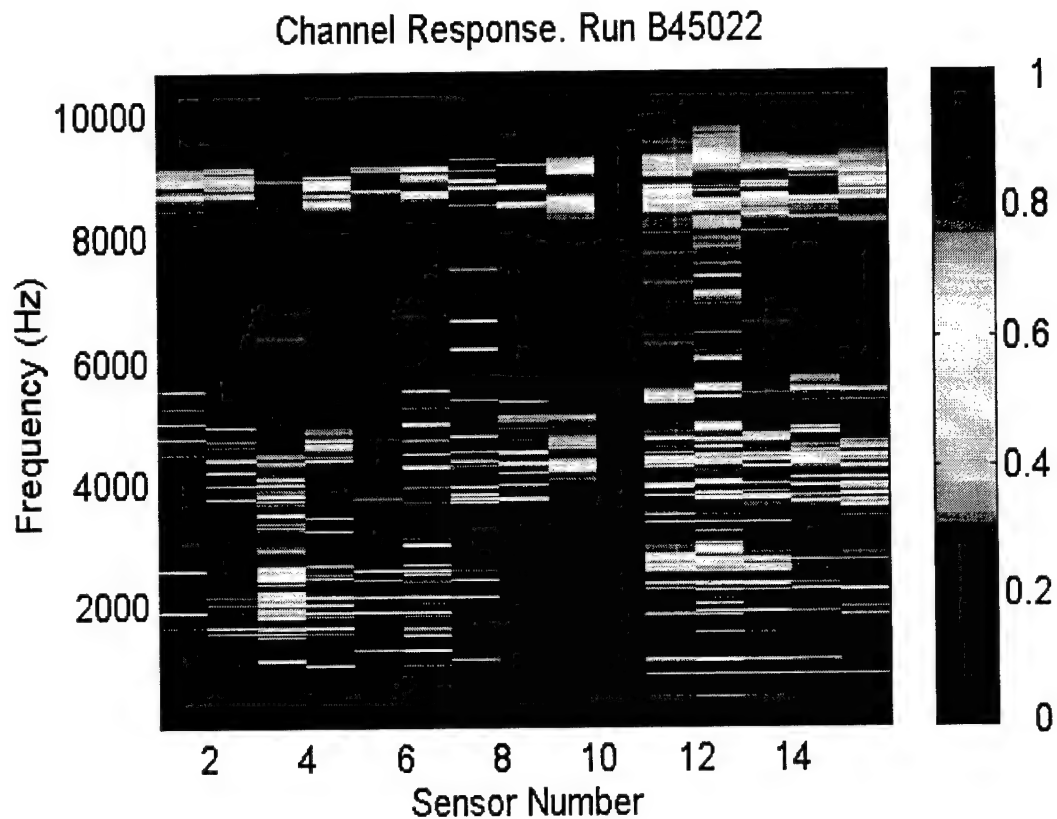


Figure 3-5: Channel response characteristics for run bare hull run B45022 taken at 450 feet.

A key structural characteristic of a finite, ring stiffened cylinder is the ring frequency which is defined as:

$$f_R = \frac{1}{2\pi r} \left[\frac{E}{\rho(1-\nu^2)} \right] \quad (3.4)$$

The ring frequency is a measure of the breathing mode of the cylinder. The breathing mode describes the expansion and contraction of the shell in a radial direction. An examination of the equation yields the observation that the equation does not make any reference to any stiffeners added to the shell. The ring frequency represents the point where below this frequency ($f_R = 1513$ Hz), the

cylinder's damping behavior is considered to be mass controlled. Above this frequency, the response is considered to be stiffness controlled. The calculation of this ring frequency also does not include the effects of added mass. Added mass, caused by the cylinder's expansion and contraction in water, reduces the natural frequencies of the ring. Offsetting added mass effects are increases in structural stiffness attributed to frames, bulkheads and changes in hydrostatic pressure.

Given the fact that the shaker is mounted to a frame's flange section, the generated compressional wave travels through the web and produces both a flexural and longitudinal impulse on the shell. Since the cylinder radiates in water, no shear wave is introduced. Of the two waves, the radial wave dominates due to the direction of the shakers motion.

From Chapter 2, it was noted that accelerometer power is a function of longitudinal position. Frames provide a change in structural impedance which acts to either pass or stop waves as a function of frequency. These bands are important in traveling wave solutions for higher frequencies, namely for solutions to Bloch wave numbers. The Bloch wave number is defined between $\pm \frac{\pi}{d}$ where d represents the distance between equally spaced frames. Using this analysis for the Nyquist Bloch wave number ($\frac{\pi}{d}$) a corresponding frequency of 41.8 kHz is calculated. Calculation of the Bloch wave number uses the longitudinal speed ($c = 5312$ m/sec) calculated using simple plate theory for titanium. Hodges [14] [15] shows that for a given mode of propagation along the cylinder one gets a stop band every time the axial length scale of the response fits the rib spacing. Therefore, there is one near the frequency where a half-wavelength along the cylinder fits between two ribs, then again when two half-wavelengths fit and so on. Rings provide a degree of freedom such that if the shell were restrained, the

ribs would oscillate much like a cantilever. Using this background, we can extend this reasoning to include the effects of the bulkheads and stringers. Like the frames, the bulkheads and stringer section provide stiffness and a perpendicular obstruction to the axial wave. Using a half wavelength with respect from the shaker to the instrumentation bulkhead ($\lambda = 28$ inches) and the longitudinal wave speed, a Bloch frequency of 7469 Hz is calculated. Since this number is calculated for measurements referenced from the instrument bulkhead, a slightly higher value can be postulated if the effects of longitudinal stiffeners are not discounted. Though these stiffeners are not perpendicular to axial waves, their close circumferential spacing (4 inches) may give an effect similar to the frames. Reducing the half wave length to 20 inches (distance from stringer to shaker) would produce a Bloch frequency upper bound of 10.5 kHz. From figure 3-5 a large resonance peak occurs at 8.8 kHz, which may be caused by this half wave length being reflected near the bulkhead sections.

Again referring to Figure 3-5, hydrophone channel responses for 8800 Hz are elevated when compared to any of the accelerometer channels. This elevated far field response can be explained by considering the flexural wave speed compared to the speed of sound in water. Again using simple plate theory [1] the transverse (flexural) wave speed can be calculated using:

$$C_T = (\omega \kappa C_L) \quad (3.5)$$

where κ is the radius of gyration. Using the height of the frame flange (1.5 inches), κ is calculated as 0.432 inches. Above 5.82 kHz, the radial wave speed exceeds the speed of sound in water therefore displaying supersonic behavior. Responses above this frequency range should be more visible at the hydrophones.

3.3 Coating effectiveness as a function of hydrostatic pressure

Coating effectiveness is calculated by comparing the responses measured during the bare hull runs with those of the coated runs. Coating was applied to both the shell and bulkhead surfaces. Accounting for small gaps between coating sheets and gaps around instrumentation interfaces, coverage was estimated at 87.4 percent of the surface area [Appendix A]. The predicted material properties, as described in Chapter 1, include:

1. Coating reduces far field response under constant forcing.
2. Coating reduces transfer function.
3. Coating effectiveness decreases with depth due to collapse of microscopic air bubble fillers.
4. Coating effectiveness decreases below some cutoff frequency.

For each configuration, multiple runs were taken for each of the operating depths. Table 3-1 summarizes the number of runs taken for each depth along with problems, if any, encountered during data acquisition. The run name convention uses the following nomenclature; P denotes 'processed' data that was acquired and digitized using the procedures outlined in Section 3.2, the letter B or C denotes Bare or Coated configuration data respectively, subsequent numbers define the depth data was taken and the run number. As an example, PB45022 can be translated as **P**rocessed data for **B**are Hull Configuration taken at **450** Feet with the run being number **22**.

Table 3-1: Data acquisition summary for runs used during lake test program.

Bare Hull Configuration		
<u>Depth(ft)</u>	<u>Run Numbers</u>	<u>Notes:</u>
50	PB501-PB506	All runs used. Channel 13 (Hydrophone 3) data not used. (zero response).
	PB507-PB510	All runs and channels used.
200	PB2001-PB20010	All runs and channels used.
450	PB4501-PB45021	21 runs taken due to poor weather at Yellow Barge (wind). Channel 13 data not used. (zero response). Channel 14 (Hydrophone 3) response from 1 kHz to 4 kHz was not consistent with the other hydrophones given a elevated response for that frequency range. Response therefore not used for these runs.
	PB45022-PB45026	All runs and channels used.
Coated Hull Configuration		
<u>Depth (ft)</u>	<u>Run Numbers</u>	<u>Notes:</u>
50	PC501-5010	All runs and channels used.
200	PC2002-PC2010	All runs and channels used
450	PC4501-PC45010	PC4502 incorrectly labeled. No data acquired for this run. (9 total runs used)

Each run was collected and compared to ensure tracking. Windy lake conditions required the collection of extra data runs to guard against the possibility that the cylinder's beam was no longer aligned to the vertical line array. A simple average of those responses were compared to the median

response. Since average response differed from the median by less than 2 dB, all runs were used for averaging purposes. Using Table 3-1 parameters, each run was both noise and force corrected prior to averaging. dB powers were converted to absolute power then averaged over the number of runs and sensors used. From this data, the following information is calculated, namely:

- Accelerometer response (coated and uncoated). [Figures 3-6 a through c]
- Hydrophone response (coated and uncoated). [Figures 3-7 a through c]
- Coating effectiveness. [Figures 3-8 a through c]
- Bare and coated Transfer Functions. [Figures 3-9 a through c]

The calculation of transfer functions, represents a difference in the frequency response using a linear filter treatment. Since we are using dB power, the calculation of the transfer function is greatly simplified as defined by the following:

$$F_{H/A}(f) = 10 \log_{10} \frac{\sum_{j=1}^n \left\{ \frac{1}{m} \sum_{k=1}^m H_k^B \right\}}{\sum_{j=1}^n \left\{ \frac{1}{r} \sum_{k=1}^r A_k^B \right\}} \quad (3.6)$$

where n denotes the number of runs, m denotes the number of hydrophones averaged over a particular run, r denotes the number of accelerometers averaged for the run. For the coated frequency response, the same equation applies except that we now use the hydrophones and accelerometers particular to the coated runs. Since coating effectiveness is a far field response function only, the definition becomes:

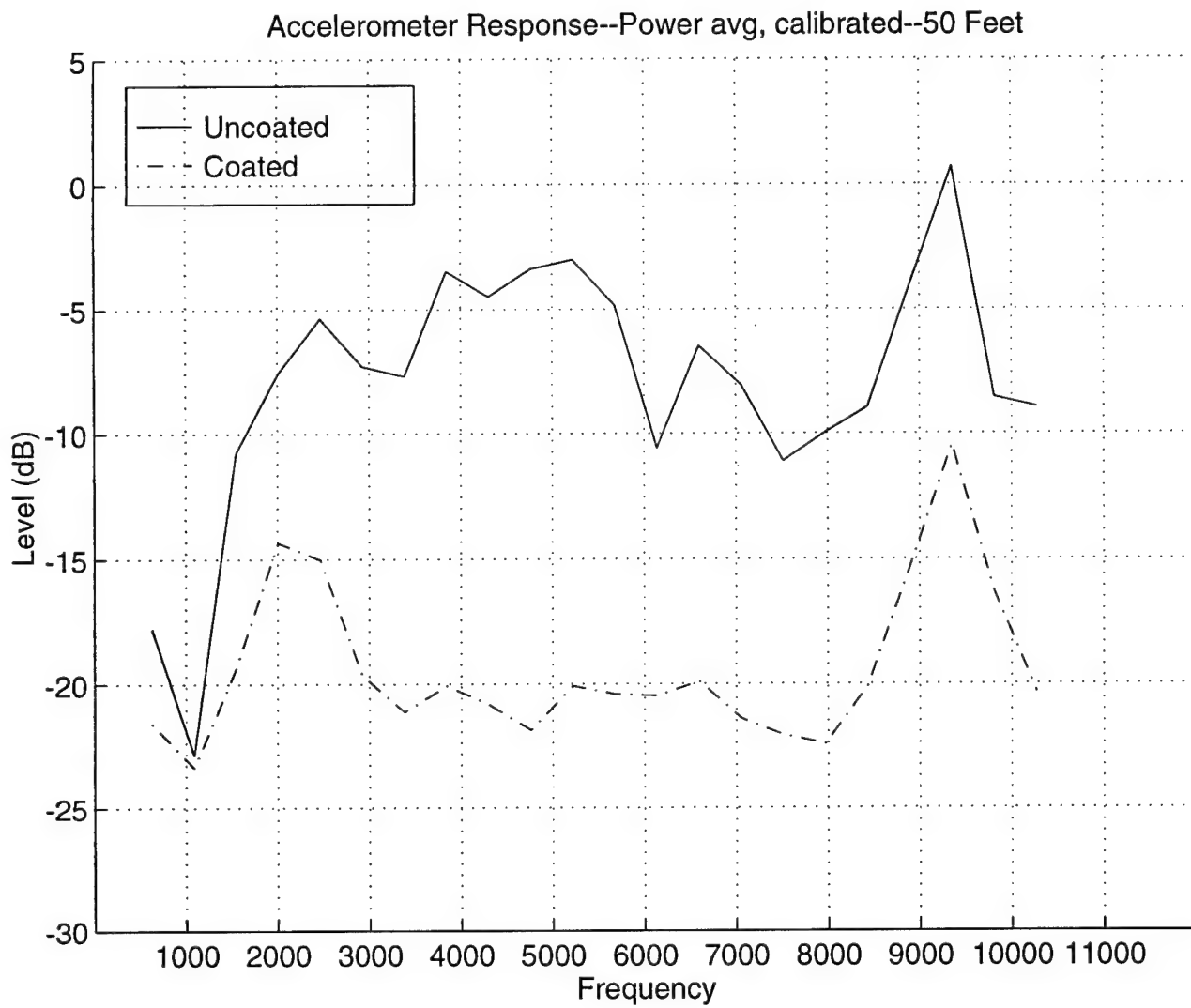


Figure 3-6 (a) : Accelerometer response (coated and uncoated). 50 feet.

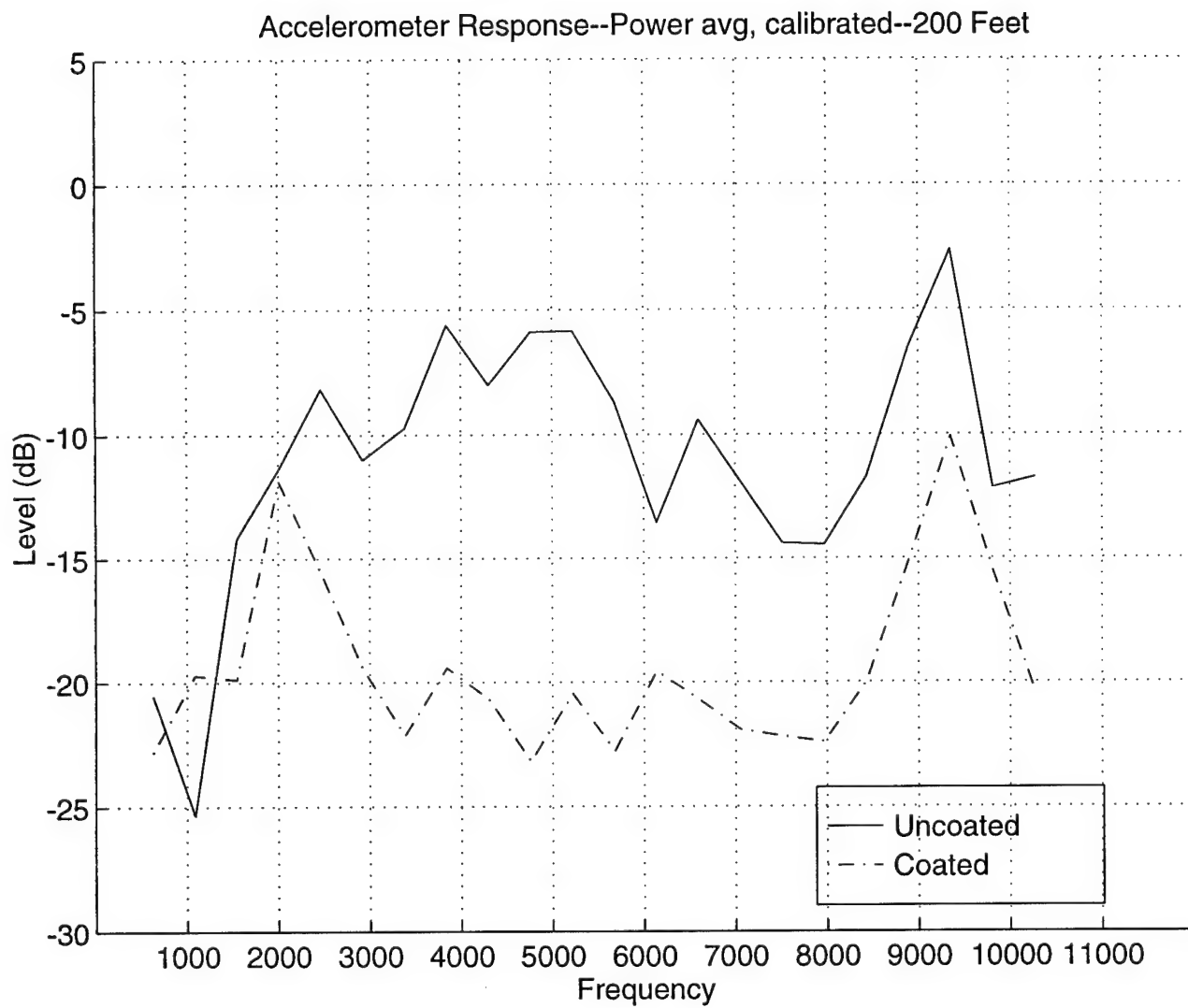


Figure 3-6 (b) : Accelerometer response (coated and uncoated). 200 feet.

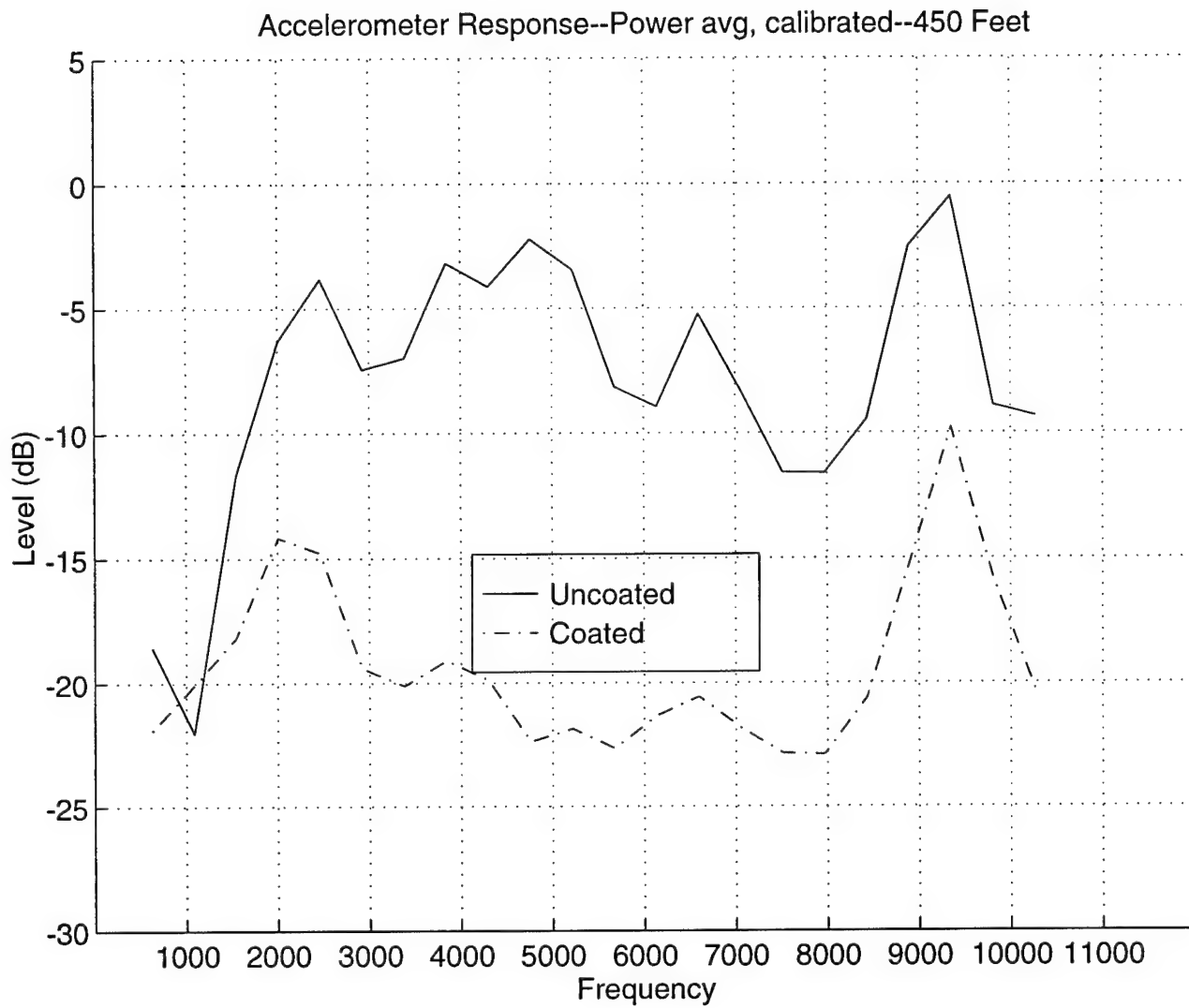


Figure 3-6 (c) : Accelerometer response (coated and uncoated). 450 feet.

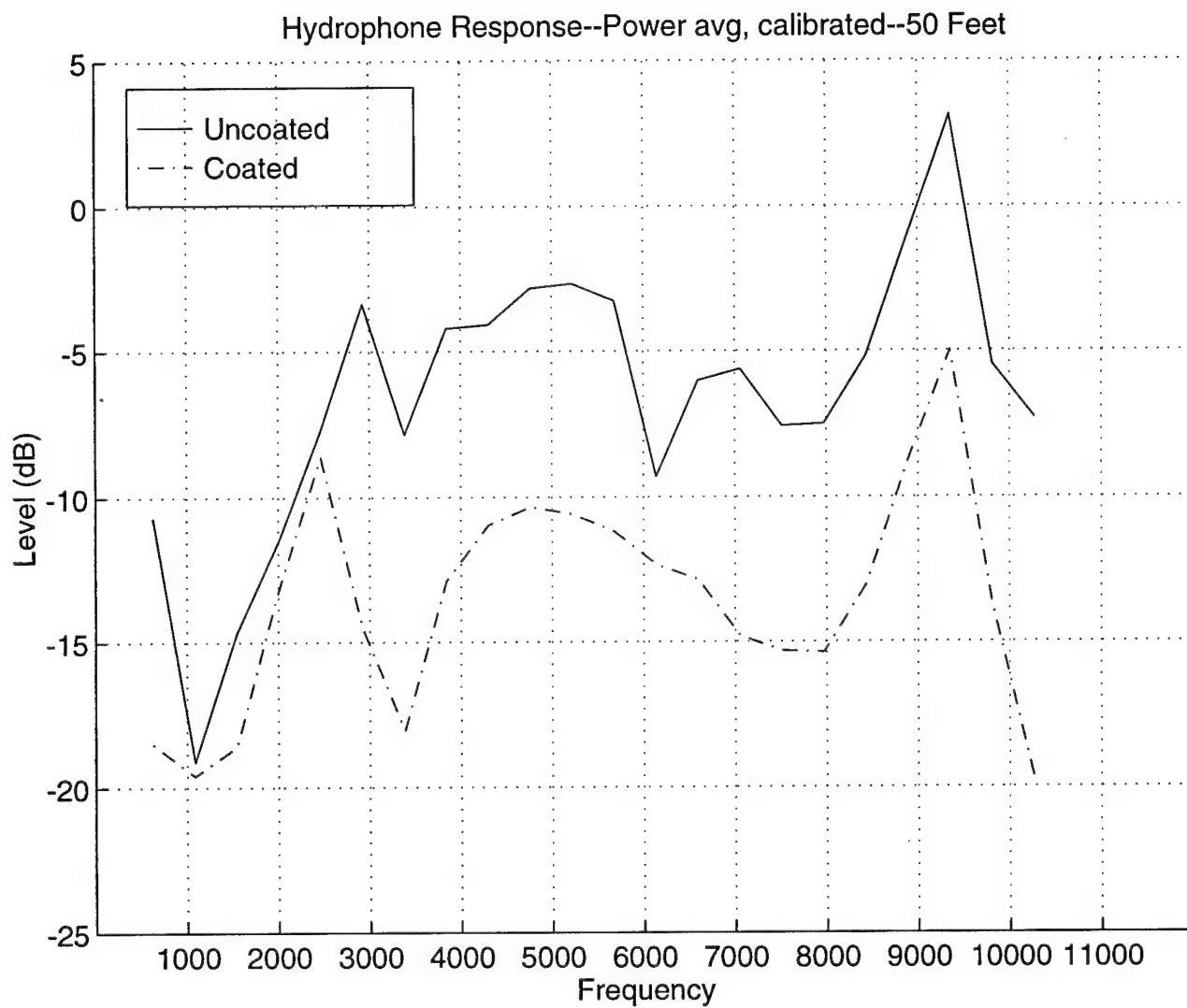


Figure 3-7 (a) : Hydrophone response (coated and uncoated). 50 feet.

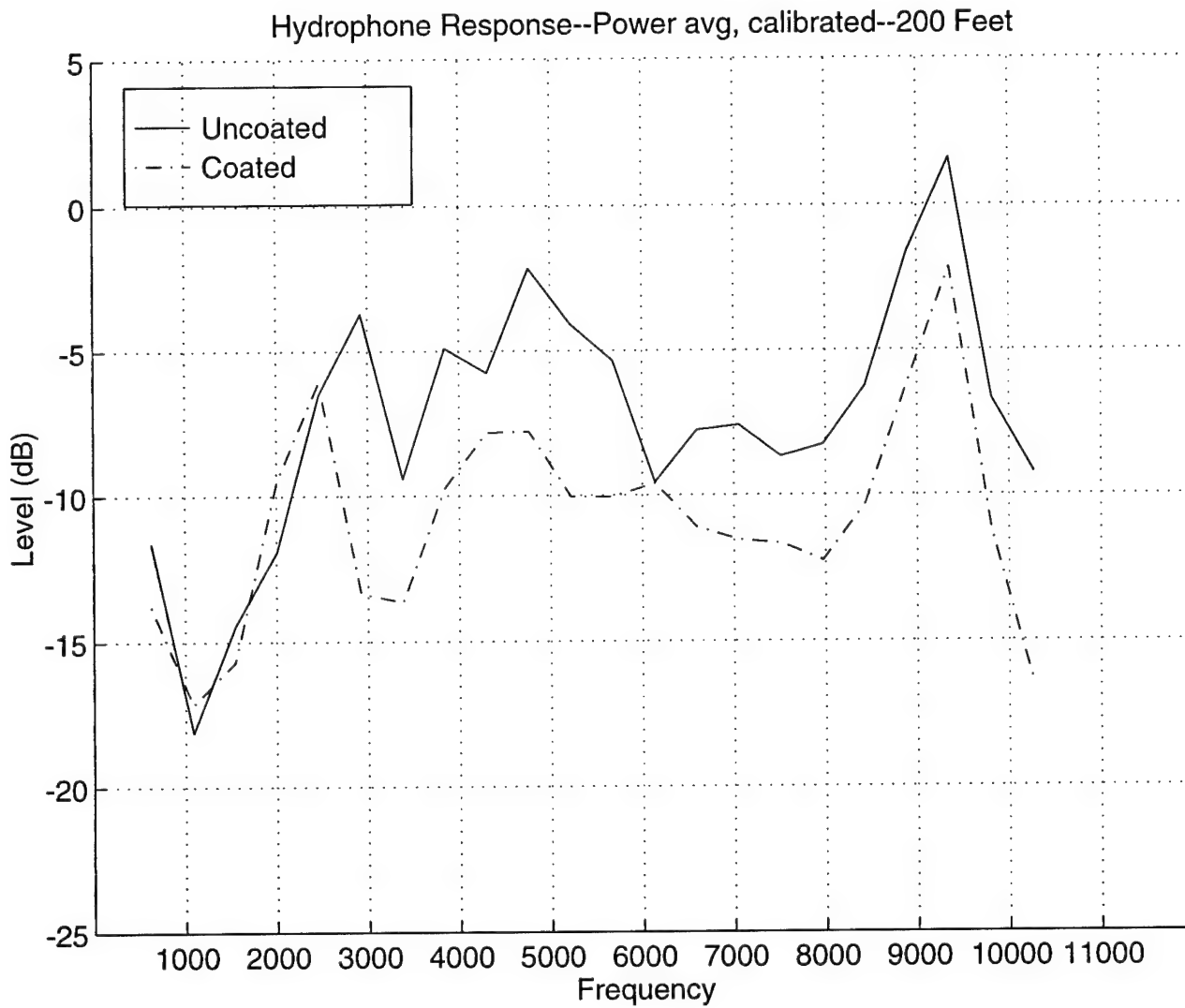


Figure 3-7 (b) : Hydrophone response (coated and uncoated). 200 feet.

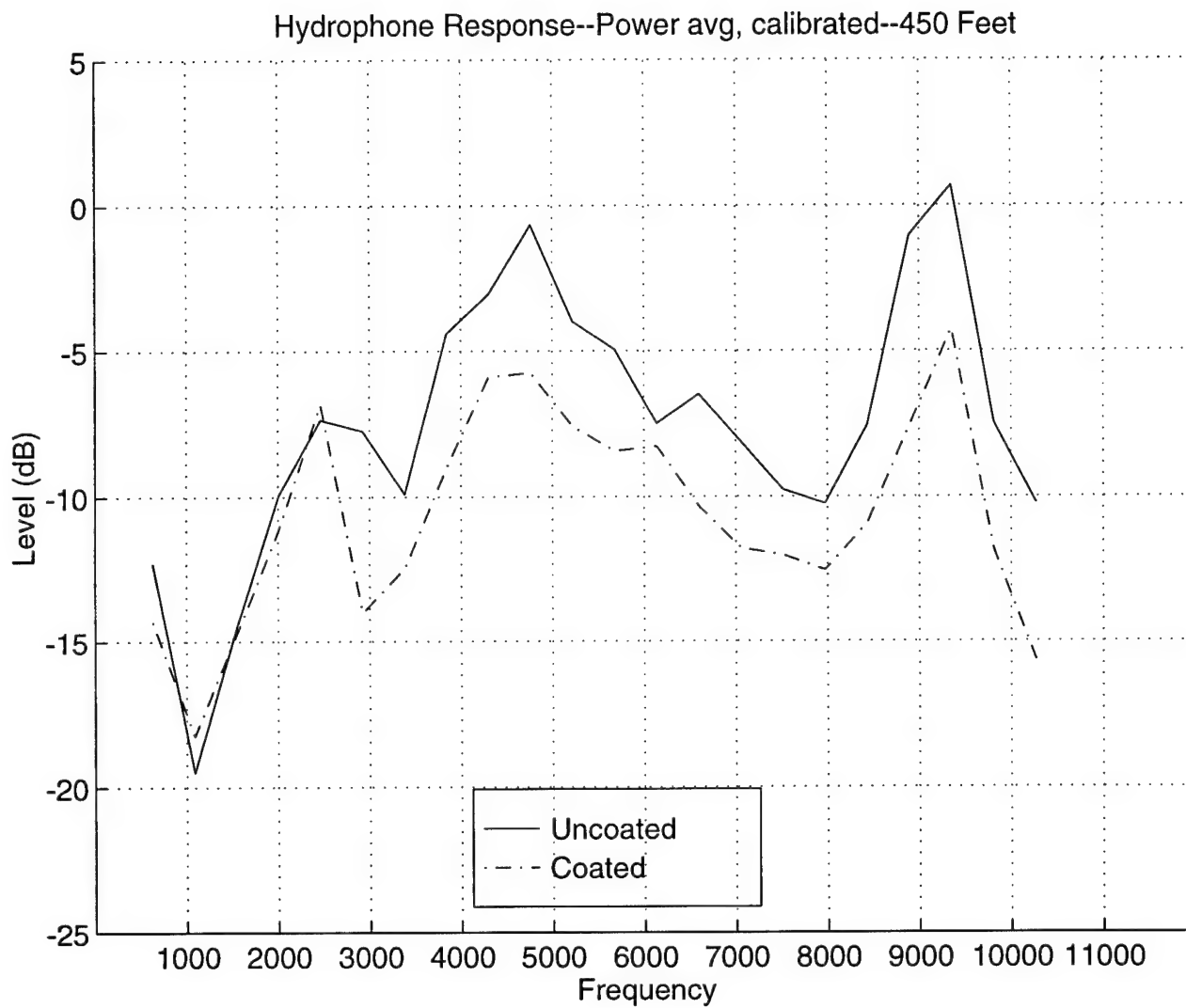


Figure 3-7 (c) : Hydrophone response (coated and uncoated). 450 feet.

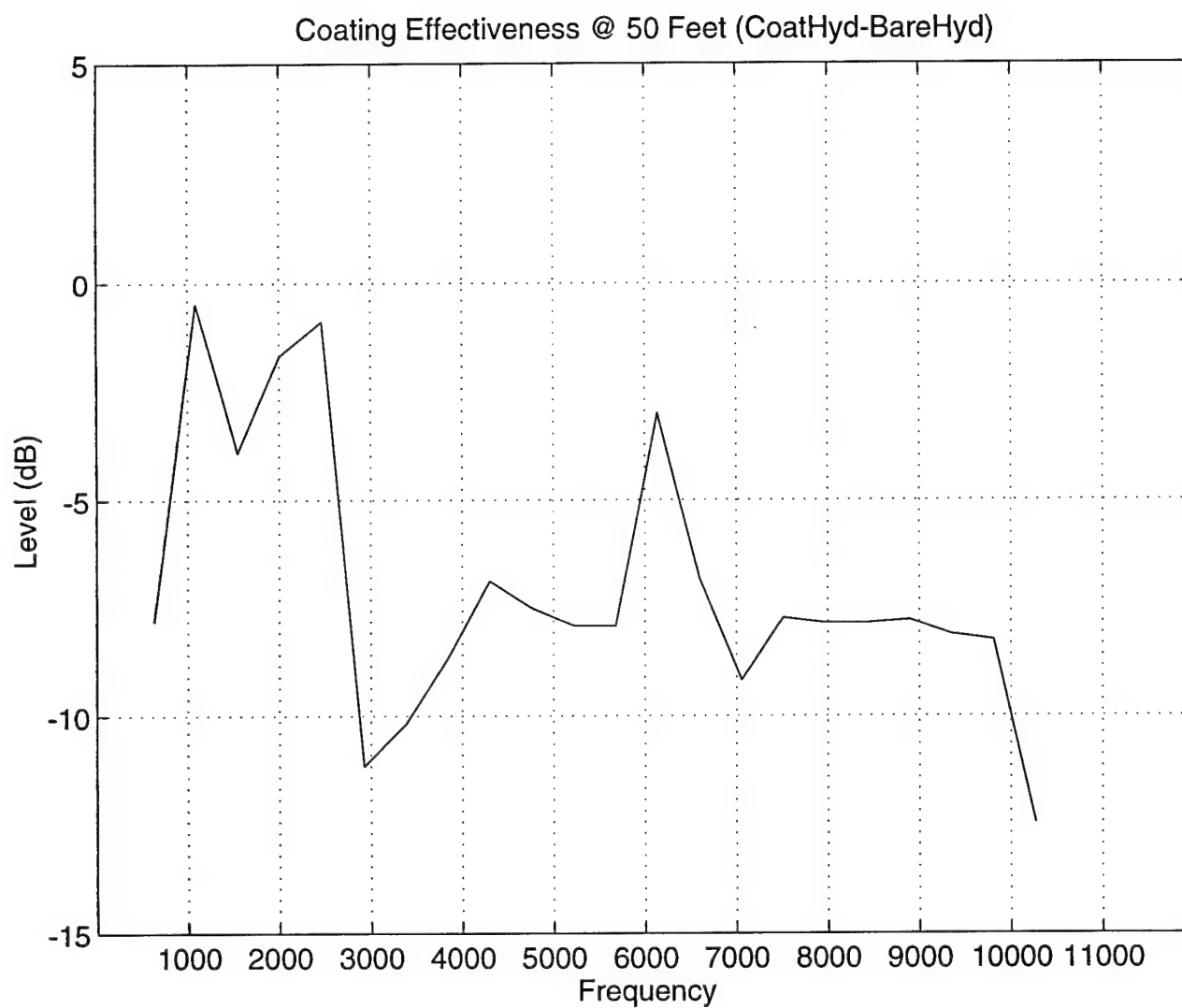


Figure 3-8 (a) : Coating effectiveness. 50 feet.

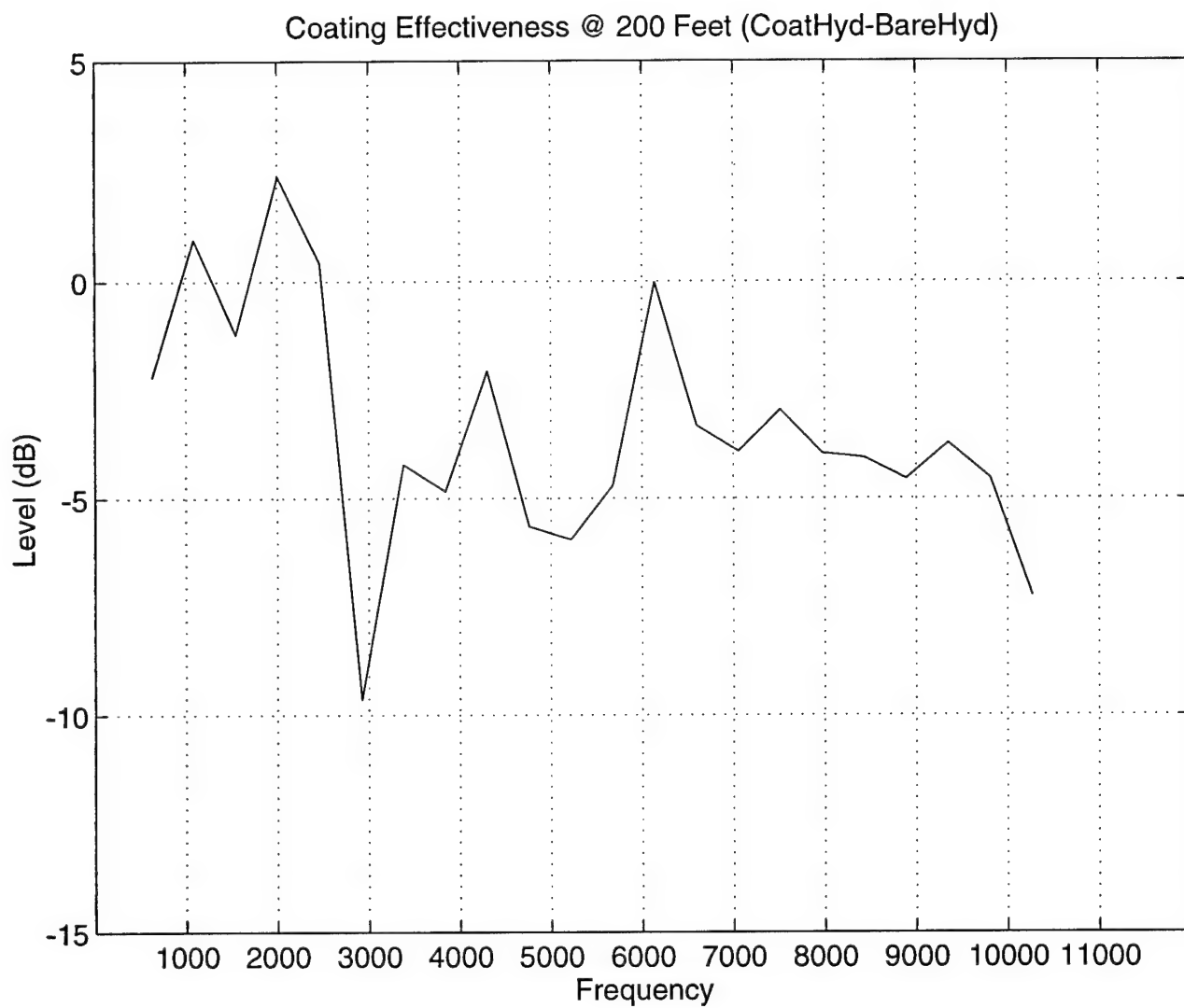


Figure 3-8 (b) : Coating effectiveness. 200 feet.

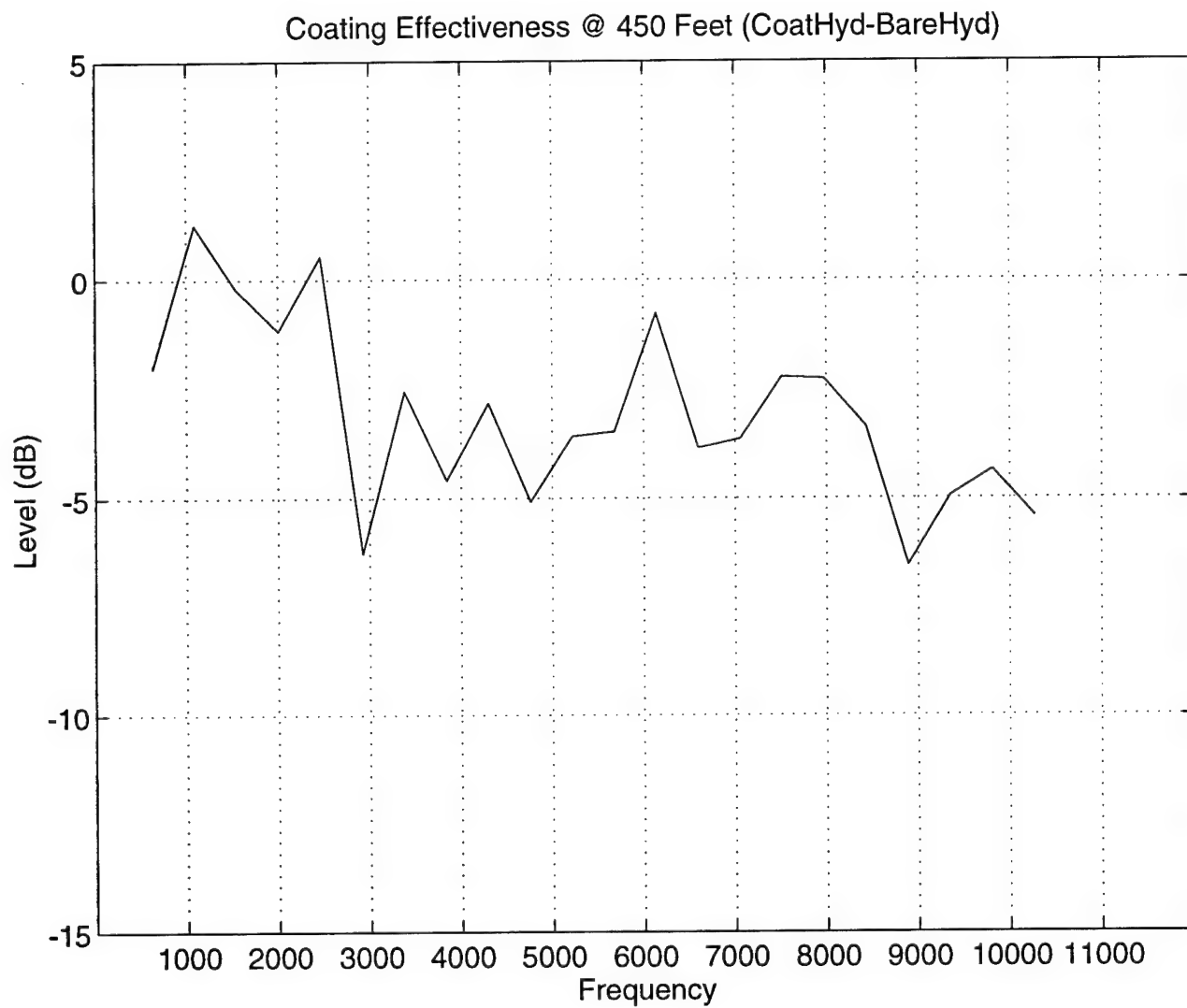


Figure 3-8 (c) : Coating effectiveness. 450 feet.

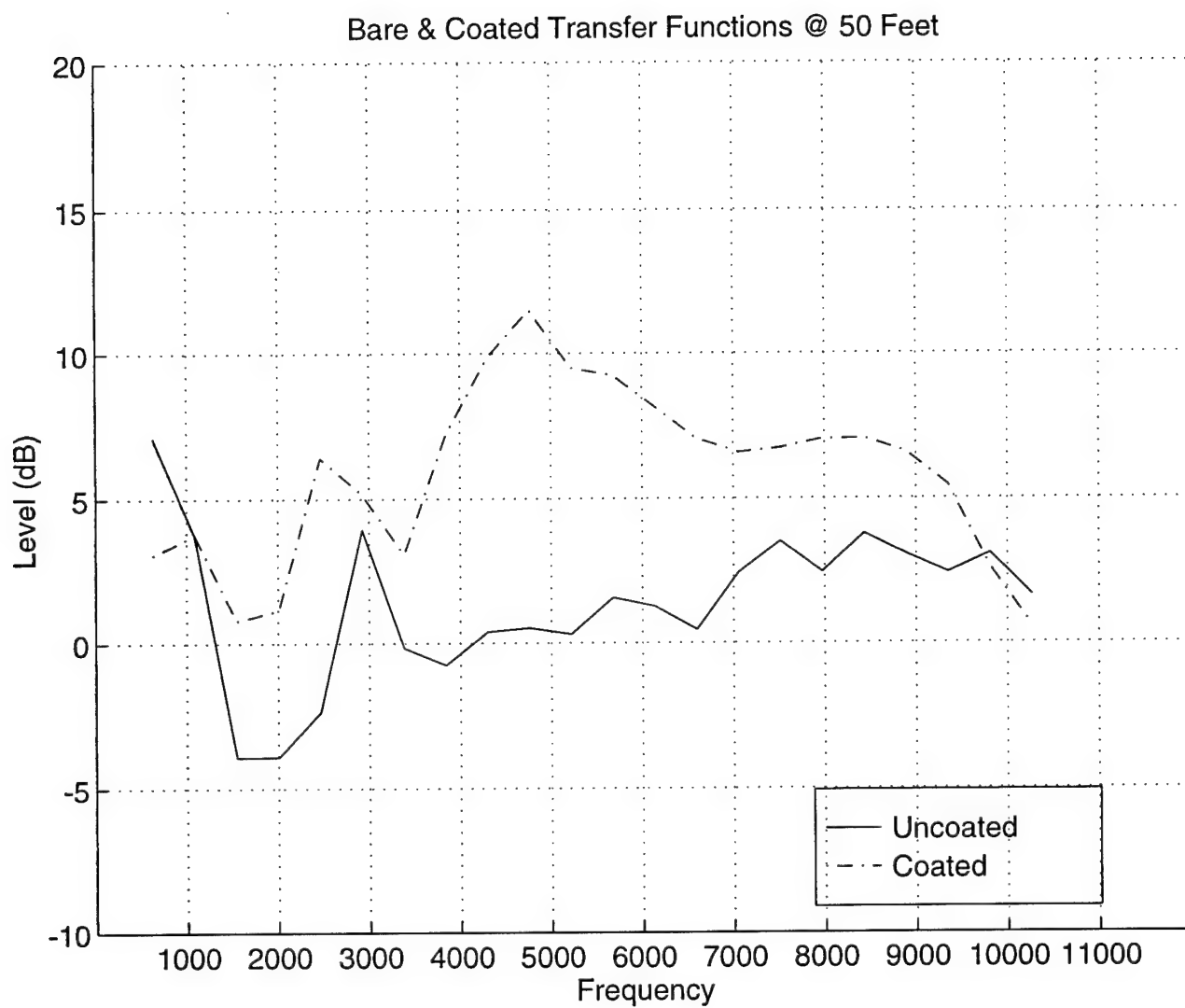


Figure 3-9 (a) : Bare and Coated Transfer Functions. 50 feet.

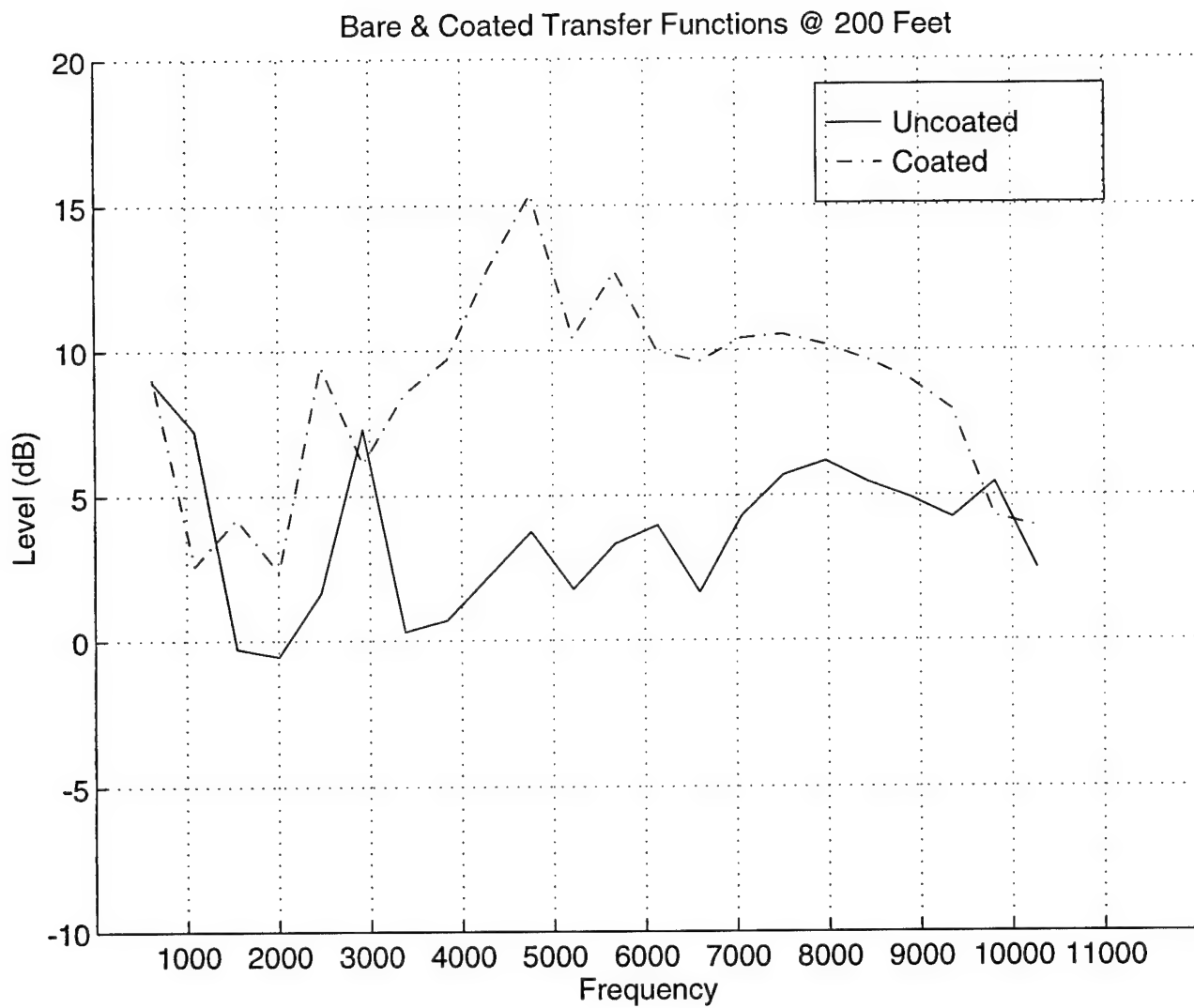


Figure 3-9 (b) : Bare and Coated Transfer Functions. 200 feet.

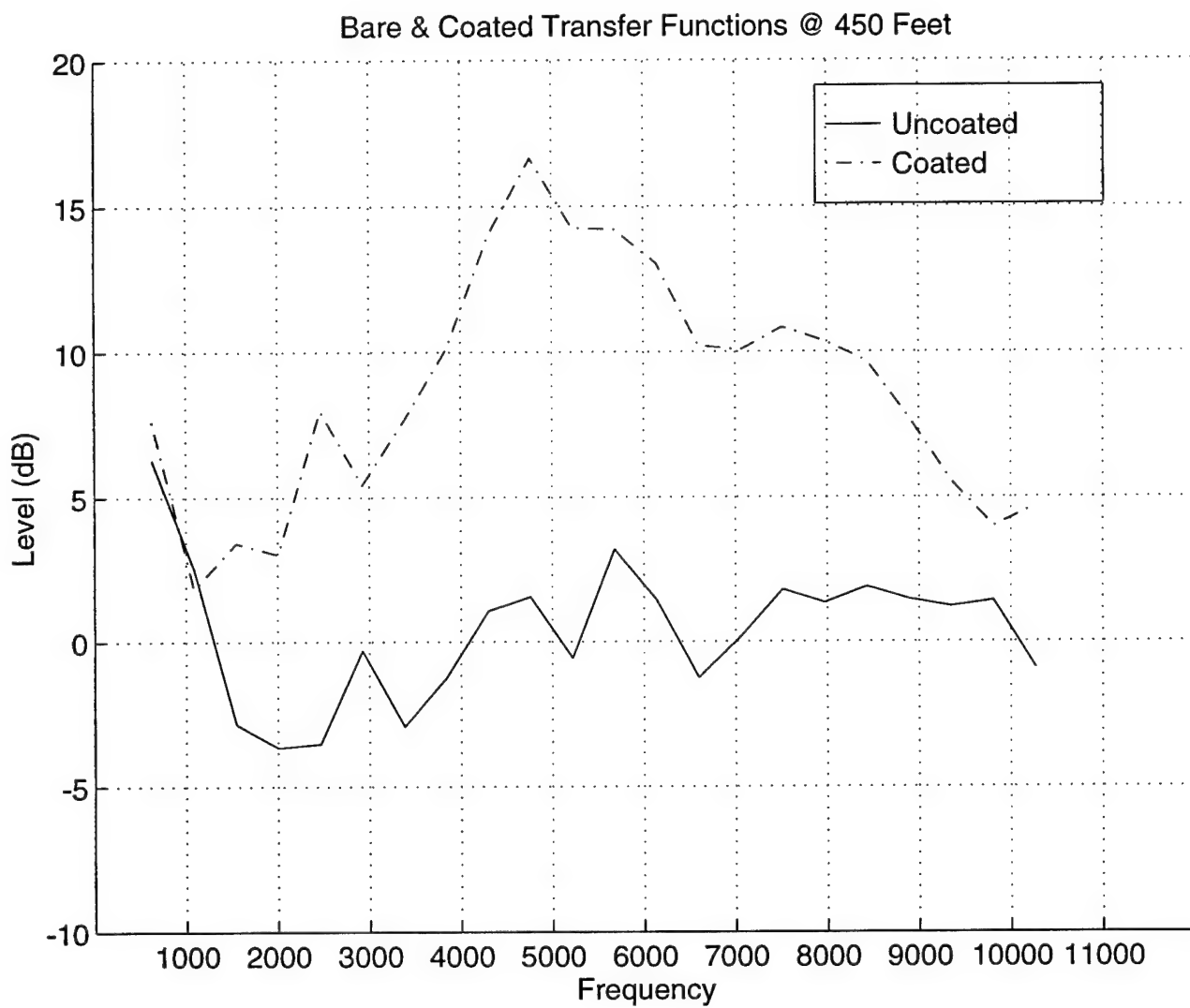


Figure 3-9 (c) : Bare and Coated Transfer Functions. 450 feet.

$$F_H = 10 \log 10 \frac{\left\{ \sum_{j=1}^r \left(\frac{1}{m} \sum_{i=1}^m H_i^C \right) \right\}}{\left\{ \sum_{k=1}^s \left(\frac{1}{n} \sum_{j=1}^n H_j^B \right) \right\}} \quad (3.7)$$

where r, s denote the number of runs for each individual configuration and m, n denotes the number of hydrophone channels used during any individual run. Because the number of hydrophones might vary between runs a weighted average was used accounting for the differences in averages due to weighting either 4 or 5 hydrophones in any given run. A sample of the data reduction MATLAB script (H_450A.M) used for calculating the responses for 450 feet are provided in the MATLAB Appendix [B].

3.3.1 Results

Since the experiment does not identify the chemical composition, what follows is a general discussion of results for standard polymeric coatings. Recall, coating effectiveness is a function of temperature, frequency, molecular structure of the base polymer, chemical cross-linking systems and filler materials. This experiment only varies frequency and filler materials (collapse of microscopic air bubble through hydrostatic pressure). Since the coating is thin, we rely on air bubbles to transform longitudinal waves into highly attenuated shear waves thereby reducing far field signature. With increasing hydrostatic pressure, the coating effectiveness is reduced due to this collapse of this bubble. At 50 feet, the maximum effectiveness is achieved. For frequencies above 3 kHz, a 7 to 8 dB reduction is noted. Not all this reduction is believed to be coating related. Some reduction may be due to the instrumentation geometry. With the array's top hydrophone within 38 feet of a pressure release surface, some phase cancellation may be apparent. Pressure release surfaces occur where there is

sharp change in impedance such as the water / air interface. At this interface, reflection occurs and may contribute to some reduction in the received hydrophone power. To examine this effect, the coated responses at 50 feet were force and noise corrected then plotted out to see if the hydrophone # 5 response showed any visible signs of phase cancellation.

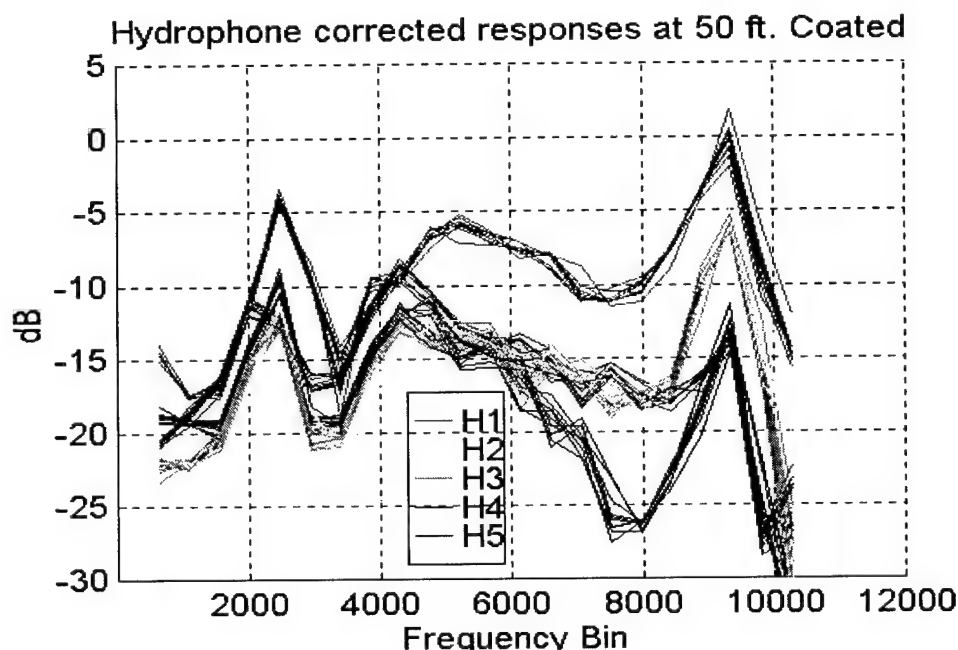


Figure 3-10: Comparison of hydrophone responses at 50 feet. All hydrophones are both force and noise corrected. Hydrophone 5 response is the lowest grouping of lines at 8 kHz

Using this graphic, some signal loss is apparent at hydrophone number 5 which is nearest to the surface. However, a comparison of the signals from the other depths (200 feet and 450 feet) show a similar trend where hydrophone 5's signal is the lowest. Since the array is closely spaced, small errors in the hydrophone arrays actual depth will not make any large differences except for the first depth (50 feet) where a 6 foot error in array depth could make for some phase cancellation.

Coating effectiveness for both 200 and 450 feet, provide a 3-5 dB reduction in far field signal strength. Increasing hydrostatic pressure does not make any noticeable changes from 200 to 450 feet.

3.3.2 Transfer function results

Transfer Function results offer a paradox. From the definition of the transfer function, or more correctly the frequency response function, this measure provides a ratio between an output signal (hydrophones) to an input signal (accelerometers). With a dampening (loss) treatment, a negative dB transfer function would be expected per the linear filter treatment. Since a positive response is measured, the implication is that the amount of structural dampening is greater than the reduction in far field. Coating, coupled with increasing hydrostatic pressure, increases structural dampening.

An implicit assumption made with this model is that the input power to the filter is a constant value and that sufficient sensors exist that accurately gage this power. An accurate gage of input power requires knowledge of the coating's velocity since flexural movement of the shell (titanium) and the coating are at different rates due to the bulk properties of each material. Power approximations are also a function of the number, placement and averaging techniques used. Small errors were introduced by utilizing a straight average of all accelerometer channels. Since power varies longitudinally for our accelerometer setup, this averaging scheme introduces errors since power generation is greatest in the

first three neighboring bays adjacent to the shaker. To gauge this error consider the bare hull transfer function values for each of the depths. For each of the depths, the transfer functions are slightly positive between 2-4 dB above 3 kHz. With hydrophones measuring a far field response, we can expect output power levels to be accurately measured.

Chapter 4

Conclusions

The change in frequency response, or transfer functions, were experimentally determined for a coated, ring stiffened cylinder as a function of hydrostatic pressure. Coating behavior can be summarized as follows:

1. Far field response is reduced for constant forcing. Application of coating provided a 5-8 dB far field reduction for 50 feet and a 3 dB reduction for both 200 and 450 feet. Reduction can be attributed to conversion of longitudinal waves into shearing waves inside the coating at the microbubble interface
2. Effectiveness decreases with depth. These same microbubbles lose their effectiveness as hydrostatic pressure collapse the bubble's radius. Since increasing depth from 200 feet to 450 feet produced no notable differences, further changes in hydrostatic pressure may also produce similar 3 dB reductions.
3. Application of coating increases the transfer function as defined as the quotient of the far field response change with respect to the accelerometer input power. Structural dampening changes attributed to both the coating and increased hydrostatic pressure increasing stiffness create a larger change in the input power compared to hydrophone far field response thereby producing a positive change in the transfer function. Transfer function changes are therefore misleading in regard to the coating effectiveness. Coating effectiveness measures (Figures 3-8 (a) through (c)) should be considered the gage of coating performance.
4. Coating performance improved significantly above a threshold of 3 kHz. Using a longitudinal wave speed of 5312 m/sec a wavelength of 1.76 meters (5.7 feet) is calculated. Since this length corresponds to the characteristic length of the cylinder (5 feet), the implication is that for frequencies below 3

kHz, the wavelength is too long to realize any effective loss mechanisms attributed to the coating.

References:

1. M.C.Junger and D.Feit, Sound, Structures and Their Interactions, 2nd Edition, The MIT Press, Cambridge, MA, 1986
2. H. Schmidt, "Numerically stable global matrix approach to radiation and scattering from spherically stratified shells". *J. Acoustic. Soc. Am.*, 94(4):2420-2430, 1993
3. D.C. Ricks and H. Schmidt, "A numerically stable global matrix method for cylindrically layered shells excited by ring forces", *J. Acoustic. Soc. Am.*, 95(6):3339-3349, 1994.
4. *SARA-2D Operators Guide*. BBN. New London, CT (1995)
5. Sound and Vibration Dampening with Polymers, R.D. Corsaro and L.H. Sperling, editors. ACS Symposium Series 424.
6. S.Kanapathipillai and K.P. Byrne, "Effects of a porous jacket on sound radiated from a pipe", *J. Acoustic. Soc. Am.*, 100(2):882-888, 1996.
7. B.H. Houston, M.H. Marcu, J.A. Bucaro, E.G. Williams, and D.M. Photiadis, "The structural acoustics and active control of interior noise in a ribbed cylindrical shell", *J. Acoustic. Soc. Am.*, 99(6):3497-3512 (1996)
8. L. Cheng, "Fluid-structural coupling of a plate-ended cylindrical shell: vibration and internal sound field," *J. Sound Vibration*. 174, 641-654 (1994)
9. *Vibration Generating System Operating Guide. Model F7/F4 Shaker*. Wilcoxon Research. Rockville, MD (1/89)
10. Conversation with Alex Edsall, Draper Labs UUV division head (9/96)
11. Pierce, A.D. "Acoustics-An Introduction to Its Physical Principles and Applications", 2nd ed. , McGraw-Hill, Inc., Woodbury, New York, 1991
12. S. Park, "*Sound Wave Scattering by Cylindrical Shells with Internal Structures*", MSOE Thesis, Massachusetts Institute of Technology (2/95)
13. "Stress Analysis of UUV1 D Hull Bulkhead" test memorandum. Charles Stark Draper Laboratory. Memo No. E21-97-0147 of 14 Feb 97.
14. Ziomek, L.J. "Fundamentals of Acoustic Field Theory and Space-Time Signal Processing", CRC Press, Inc., Boca Raton, Florida, 1995
15. C.H. Hodges, J. Power and J. Woodhouse, "The low frequency vibration of a ribbed cylinder, Part 1: Theory" ,*J. Sound Vibration*. 101(2), 219-235 (1985)
16. C.H. Hodges, J. Power and J. Woodhouse, "The low frequency vibration of a ribbed cylinder, Part 2: Observations and Interpretation" ,*J. Sound Vibration*. 101(2), 219-235 (1985)

Appendix A: Ring stiffened cylinder coating effectiveness worksheet

Experimental Constants: LTON = 2200·lbf ORIGIN = 1

Properties of Freshwater (assume lake is homogeneous medium, freshwater):

$$c_{\text{water}} = 1460 \cdot \frac{\text{m}}{\text{sec}} \quad \rho_{\text{water}} = 62.4 \cdot \frac{\text{lbf}}{\text{ft}^3}$$

Properties of Titanium (6A1-4V):

Reference: (a) Draper Lab's and (b) www.titanium.com/about.htm

$$E_T = 16.5 \cdot 10^6 \cdot \frac{\text{lbf}}{\text{in}^2} \quad \rho_T = 4.43 \cdot 10^3 \cdot \frac{\text{kg}}{\text{m}^3} \quad \nu = 0.3$$

$$c_L = \left[\frac{E_T}{\rho_T \cdot (1 - \nu^2)} \right]^{0.5}$$

Approximate speed of sound using speed of sound of a longitudinal wave in an elastic plate [Junger & Feit].

$$c_L = 5.312 \cdot 10^3 \cdot \text{m} \cdot \text{sec}^{-1}$$

Properties of Aluminum (6061-T6)

$$E_A = 10.5 \cdot 10^6 \cdot \frac{\text{lbf}}{\text{in}^2} \quad \rho_A = 2.7 \cdot 10^3 \cdot \frac{\text{kg}}{\text{m}^3} \quad \nu = 0.3$$

Frequency Pass Band:

$$f_{\text{low}} = 400 \cdot \text{Hz} \quad f_{\text{high}} = 10500 \cdot \text{Hz}$$

Cylinder Dimensions:
(w / 2 inch bulkheads)

$$L_{\text{cyl}} = 64 \cdot \text{in} \quad D_{\text{cyl}} = 44 \cdot \text{in} \quad r_{\text{cyl}} = \frac{D_{\text{cyl}}}{2} \quad n_{\text{bays}} = 10 \quad d_{\text{ring}} = 5 \cdot \text{in}$$

A. Fraunhofer Far Field Determination:

Based on the geometry of the source (cylinder) with a vertical line array in the FF, the closest distance at which phase-front curvature may be ignored can be defined as follows:

$$L = r_{\text{cyl}} \quad \lambda_h = \frac{c_{\text{water}}}{f_{\text{high}}} \quad \lambda_l = \frac{c_{\text{water}}}{f_{\text{low}}}$$

$$FF = \frac{L^2}{\lambda_h} \quad FF = 7.368 \cdot \text{ft}$$

The quadratic phase factor (Ziomek Eqn 6.2-37) can be considered insignificant if much less than 1, so:

Note: Hydrophone 3 is 25 feet from shell to hydrophone. Line array hydrophones spaced 6 feet apart.

$$r = \left[\left(25 + \frac{22}{12} \right)^2 + 12^2 \right]^{.5} \cdot \text{ft} \quad r = 29.394 \cdot \text{ft} \quad r_o = 22 \cdot \text{in}$$

$$QPF = \frac{\pi \cdot r_o^2}{\lambda_h \cdot r} \quad QPF = 0.787$$

$$b = \left(\frac{r_o}{r} \right)^2 \quad b = 3.89 \cdot 10^{-3} \quad \text{No real phase variation between } r_o \text{ and } r \text{ so ff.}$$

Examination of FF using spherical wave criteria ($ka \gg 1$)

$$k = 2 \cdot \frac{\pi}{\lambda_l} \quad k = 1.721 \cdot \text{m}^{-1} \quad \lambda_l = 3.65 \cdot \text{m}$$

$$FF_{\text{SPHERICAL}} = k \cdot (r - r_o) \quad FF_{\text{SPHERICAL}} = 14.461$$

All calculations show that 25 feet satisfies far field criteria for this frequency range.

B. Ring Frequency Calculation (Breathing Mode Determination)

$$f_R = \frac{1}{2 \cdot \pi \cdot r_{\text{cyl}}} \left[\frac{E_T}{\rho_T \cdot (1 - \nu^2)} \right]^{.5} \quad f_R = 1.513 \cdot 10^3 \cdot \text{Hz}$$

C. Axial Bloch Wave Numbers

$$i = 1 \dots 9 \quad q_i = \frac{i}{n_{\text{bays}}} \cdot \left(\frac{\pi}{d_{\text{ring}}} \right)$$

$$q = \frac{\pi}{d_{\text{ring}}}$$

$$\lambda_B = 2 \cdot \frac{\pi}{q}$$

$$f_B = \frac{c_L}{\lambda_B}$$

$$f_B = 2.091 \cdot 10^4 \cdot \text{sec}^{-1}$$

Bloch wave numbers are used for determining resonant behavior of the frames for frequencies that are higher than the band being looked at for this experiment. Also the principal direction of radiation is radially out not in a longitudinal direction.

Determination of the flexural wave speed using plate theory....

$$f_{\text{res}} = 8700 \cdot \text{Hz}$$

$$R = 22 \cdot \text{in}$$

$$h = 1.5 \cdot \text{in}$$

Use height of the frame flange (1.5 inches) instead of just 5 using the thickness of the plate.

$$t = 0.25 \cdot \text{in}$$

$$\omega = 8800 \cdot \text{Hz} \cdot 2 \cdot \pi$$

$$\omega = 5.529 \cdot 10^4 \cdot \text{sec}^{-1}$$

$$K = 0.288 \cdot h$$

$$K = 0.011 \cdot \text{m}$$

Radius of Gyration

$$C_F = \frac{(h \cdot c_L \cdot \omega)^5}{12^{.25}}$$

$$C_T = (\omega \cdot K \cdot c_L)^5$$

$$C_F = 1.797 \cdot 10^3 \cdot \text{m} \cdot \text{sec}^{-1}$$

$$C_T = 1.795 \cdot 10^3 \cdot \text{m} \cdot \text{sec}^{-1}$$

Junger and Feit (7.63) provides the flexural velocity of a plate. Function of frequency

The characteristic distance for radial waves is around the circumference:

$$\text{Circumference} = 44 \cdot \pi$$

$$\text{Circumference} = 138.23 \cdot \text{in}$$

$$\text{Natural frequency for a pipe:} \quad L = \text{Circumference} \quad n = 1$$

$$f = \frac{n \cdot c \cdot L}{2 \cdot L} \quad f = 756.507 \cdot \text{sec}^{-1}$$

D. Calculation of wt to be added to cylinder to make it neutrally buoyant.

$$\text{Volume}_{\text{cyl}} = \frac{\pi \cdot (2 \cdot r_{\text{cyl}})^2}{4} \cdot L_{\text{cyl}} \quad \text{Volume}_{\text{cyl}} = 1.595 \cdot \text{m}^3$$

$$\text{Displacement} = \rho_{\text{water}} \cdot \text{Volume}_{\text{cyl}} \quad \text{Displacement} = 3.514 \cdot 10^3 \cdot \text{lbf}$$

$$\text{CylinderWt} = 1500 \cdot \text{lbf}$$

Measure weight of cylinder at Lake Pend Oreille

$$\text{Required_Ballast} = \text{Displacement} - \text{CylinderWt}$$

$$\text{Required_Ballast} = 2.014 \cdot 10^3 \cdot \text{lbf}$$

This number reflects the minimum ballast necessary to submerge the cylinder in freshwater. To prevent movement, an additional 700 lbf of lead ballast are added to the test cylinder rig.

E. Percentage of cylinder coated:

These measurements were made prior to submerging the coated cylinder into Lake Pend Oreille

$$\text{BodyArea} = \pi \cdot D_{\text{cyl}} \cdot L_{\text{cyl}} + \left(\frac{D_{\text{cyl}}}{2} \right)^2 \pi \cdot 2 \quad \text{BodyArea} = 71.995 \cdot \text{ft}^2$$

$$\text{BAreaUncovered} = 2 \cdot \text{ft} \cdot \frac{3}{4} \cdot \text{in} + 5.5 \cdot \text{in} \cdot 1 \cdot \text{in} + 2 \cdot \text{ft} \cdot 1 \cdot \text{in} + 5.25 \cdot \text{in} \cdot \pi \cdot D_{\text{cyl}}$$

$$\text{BAreaUncovered} = 5.369 \cdot \text{ft}^2$$

$$\text{EAreaUn1} = \pi \cdot \left(\frac{D_{\text{cyl}}}{2} \right)^2 \cdot 42 \cdot \text{in}^2 + 2 \cdot \text{in} \cdot 2 \cdot (D_{\text{cyl}} - 12 \cdot \text{in}) + 4 \cdot \pi \cdot (3.5 \cdot \text{in})^2 + \pi \cdot (6 \cdot \text{in})^2$$

$$\text{EAreaUn1} = 2.765 \cdot \text{ft}^2$$

$$\text{EAreaUn2} = \pi \cdot \left(\frac{D_{\text{cyl}}}{2} \right)^2 \cdot 42 \cdot \text{in}^2 + 2 \cdot \text{in} \cdot 2 \cdot (D_{\text{cyl}} - 12 \cdot \text{in})$$

$$\text{EAreaUn2} = 0.911 \cdot \text{ft}^2$$

$$\text{Covered} = \text{BodyArea} - \text{BAreaUncovered} - \text{EAreaUn1} - \text{EAreaUn2}$$

$$\text{Covered} = 62.95 \cdot \text{ft}^2 \quad \text{PercentCovered} = \frac{\text{Covered}}{\text{BodyArea}} \quad \text{PercentCovered} = 0.874$$

Cylinder coated to approximately 87.4 percent of the available area.

F. LFM calculations

Number of Channels:

$$N_{\text{channels}} = 16$$

Number of (+) Data Points
(Discard negative and zero):

$$N_{\text{points}} = \frac{2^{N_{\text{channels}}}}{2} \quad N_{\text{points}} - 1 = 3.2767 \cdot 10^4$$

Sample Frequency

$$F_{\text{sample}} = 25 \cdot 10^3 \cdot \text{Hz} \quad \text{Approximately 2.5 times the highest recorded frequency (10.5 kHz)}$$

Sample Window

$$T_w = \frac{N_{\text{points}}}{F_{\text{sample}}} \quad T_w = 1.311 \cdot \text{sec}$$

Propagation time from shell to furthest hydrophone (1 or 5):

$$d = r \quad d = 29.394 \cdot \text{ft} \quad \text{Determined in FF evaluation}$$

$$\text{PropagationTime} = \frac{d}{c_{\text{water}}} \quad \text{PropagationTime} = 6.137 \cdot 10^{-3} \cdot \text{sec}$$

To account for some uncertainties in position
choose a conservative time (0.01 seconds):

$$T_{\text{prop}} = 0.01 \cdot \text{sec}$$

Filter settling time (specific to instrumentation at Lake Pend Oreille)

$$T_{\text{filter}} = 0.3276 \cdot \text{sec}$$

The LFM signal time reflects these 3 variables; time to sample, time for propagation, time for filters.

$$T_{\text{LFM}} = T_w + T_{\text{prop}} + T_{\text{filter}} \quad T_{\text{LFM}} = 0.973 \cdot \text{sec}$$

$$D_P = \pi \cdot \frac{f_{\text{high}} - f_{\text{low}}}{T_{\text{LFM}}}$$

$$D_P = 3.261 \cdot 10^4 \cdot \text{sec}^{-2}$$

Deviation
Constant (8.2-27)
(Beta in PLOTRES)

$$\alpha = F_{\text{sample}} \cdot T_{\text{LFM}}$$

$$\alpha = 2.4328 \cdot 10^4$$

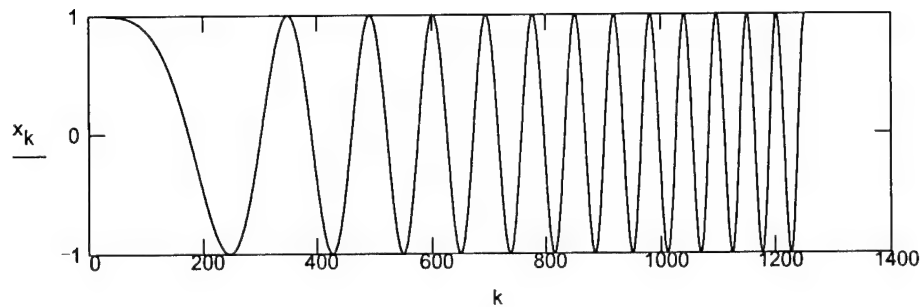
$$j = \sqrt{-1}$$

$$k = 1 \dots 1250$$

Ref: Ziomek (8.3-89)

$$x_k = \text{Re} \left[\exp \left[j \cdot D \cdot \left(\frac{k}{F_{\text{sample}}} \right)^2 \right] \right]$$

Complex Envelope for an LFM pulse
using lake instrumentation constraints
for the first 1250 points (0.05 msec)



Since the signal can not instantaneously jump to 1, we employ a cosine taper (using the MATLAB procedure PLOTSHAK, which slowly tapers up to a maximum value of 1 within 0.02 seconds.

Frequency Bin Assignments:---22 bins are used to cover the band 400 to 10.5 kHz. The center of each band is used to plot the average value of that band for the coating effectiveness portion of this experiment.

Appendix B: Matlab™ Data Acquisition and Processing Scripts

The following is a sampling of MATLAB™ scripts that were used during the experiment.

A. PLOTRES.M --The file plots the response from the 15 channels used in Figure 3-4. The file also contains the main ingredients of PLOTSHAK.M which is the data acquisition and processing script.

```
%PLOTRES.M--Plot frequency response of 15 channels
%Developed by Dr. R. Dicus (SAIC Tysons Corner, VA).
%ARD digitizer captures 32 K points.
%Sampled signal values are integer from -32768 to +32767.
%Sample rate = 25 K.
%Total sample window time is 1.3107 s.
%Lead-in time is 0.3276 s.
%Propagation time from cylinder to hydrophones will be
%approximately 5 msec (.005 s).
%We will allow .01 s for prop time.
%Actual signal time timax will then be 0.9731 s.
%Waveform will sweep from 400 Hz to 10 kHz.
%Shaker and driver require that waveform start and end at
%zero and do so smoothly.
%Set anti-alias filters to bandpass from 10 Hz to 10500 Hz.
%-----
filename='B45022'           % Unprocessed Bare Hull Run
timax=0.9731;               % Time interval for complex env.
fsample=25000;              % Sample rate to avoid aliasing
npoints=32770;              % Digitizer capture
delf=10500-400;              % Passband
beta=delf*pi/timax;         % Complex Envelope
nsensor=15;                 % 15 channels of data
deltaf=fsample/32768;       % Complex Envelope development
freq=(0:16383)*deltaf;      % Freq correlation for band
flo=400;                    % Low end
fhi=10500;                  % High end
iflo=1+round(flo/deltaf);   % Index frequency (low)
ifhi=1+round(fhi/deltaf);   % Index frequency (high)
nbin=round(delf/(22*deltaf)); % Number of points per bin
fbinedge=400+(0:22)*delf/22; % Frequency start points of bins
% -----
imax=zeros(4,nsensor);      % Pre-staging imax matrix (4 x 15)
powerbin=zeros(4,nsensor);  % Pre-staging powerbin (4 x 15)
dbpower=zeros(22,nsensor);  % Pre-staging dbpower (22 x 15)
image=zeros(14000,nsensor+1); % Pre-staging image (14000 x 16)
% -----
decimate=10;                %
imagemax=zeros(14000/decimate,nsensor+1); %
%Input data; detect start of each signal
s=['load ',filename];       % Assign B45022 to s
```

```

eval(s); % Load B45022
data=mmsdata; % Load 16 time series of data
noisetime=0.2; % Lead in time
noiselength=noisetime*fsample; % Number of samples in noise
clf; % Clear any previous figures
%smark=['*', '+', 'o', 'x', '.'];
%sline=['-', '--', '-.', ':'];
nprocess=15; % Ch-16 is the leak detector
sensornumbers=(1:nprocess); % Process each channel sep
signalforce=data(1:32768,decimate); % Force is channel 10
signalforce=signalforce-mean(signalforce); % Remove mean component
signalforcefft=fft(signalforce,32768); % Time domain to freq
indexedge0=[2000 4000 7000 11000]; % Bins for response
indexedgehi=[4000 6000 9000 13000]; % Bins for response
for processindex=1:15
    isensor=sensornumbers(processindex); % Process each sensor
    signal=data(1:32768,isensor); % Matrix to array
    signal=signal-mean(signal); % Remove mean component
    signalfft=fft(signal,32768); % Time domain to freq
    % -----
    % Normalize by force (each component)
    signalnorm=abs(signalfft(1:16384))./abs(signalforcefft(1:16384));
    signalnorm(1:iflo)=zeros(iflo,1);
    signalnorm(ifhi:16384)=zeros(16384-ifhi+1,1);
    % -----
    for ibin=1:4
        [powerbin(ibin,processindex),imax(ibin,processindex)]=max(signalnorm(indexedge0(ibin):indexedgehi(ibin)));
    end
    % -----
    signalnormplot=signalnorm/max(signalnorm);
    image(:,processindex)=signalnormplot(1:14000);
    indexmax=0;
    for ipixel=1:10:14000-decimate
        indexmax=indexmax+1;
        imagemax(indexmax,processindex)=max(image(ipixel:ipixel+decimate-1,processindex));
    end
end
clf
% -----
figure(1)
imagemax(:,nsensor+1)=imagemax(:,nsensor); % renumber
[nrow ncol]=size(imagemax);
sensornumber=(1:ncol)';
freqplot=(1:nrow)*decimate*deltat;
pcolor(sensornumber,freqplot,imagemax)
shading flat
colormap jet
colorbar
title('Channel Response. Run B45022')
xlabel('Sensor Number')
ylabel('Frequency (Hz)')
% -----
% Figure 2 is the plotting routine used for Figure 3-3

```

```

figure(2)
subplot(4,1,1),plot(mmsdata(:,2))
title('Accelerometer 2 Channel Response')
ylabel('Amplitude')
subplot(4,1,2),plot(mmsdata(:,9))
title('Shaker Accelerometer Channel Response')
ylabel('Amplitude')
subplot(4,1,3),plot(mmsdata(:,10))
title('Shaker Force Channel Response')
ylabel('Amplitude')
subplot(4,1,4),plot(mmsdata(:,13))
title('#3 Hydrophone Channel Response')
xlabel('Time Index')
ylabel('Amplitude')
%-----

```

B. H_450A.M--The file takes the processed input channel files created by PLOTSHAK / PLOTRES and then performs noise and force corrections to data runs for 450 feet. Figures 3-6, 3-7, 3-8 and 3-9 are generated from these files.

```

% H_450A.M: Response at 450 feet. Hydrophone/Accelerometer
% Created by R. Meyer (MIT)
% Values have been power averaged, calibration corrected
% For Runs B4501 through B45021 Hydrophone 13 and 14 omitted
% For Runs B45022 through B45026 All Hydrophones are included
% Weighted averages are used
% Date:21 Mar 97
clear; %clear all variables from memory
path('c:\cylinder\data\bare50',path)
path('c:\cylinder\data\bare450',path)
load pcal1
cal=dbpower;
%
%----Uncoated Analysis----
% Runs: pb4501 through pb45021.mat
addbarehydpower=0;addbareaccpower=0;hsum=0; % initialize variables
ifilev1=[1:21];
isensora=[1 2 3 4 5 6 7 8]; % Shaker accelerometer not used
isensorh=[11 12 15]; % Hydrophone 13 excluded
nsensorh=length(isensorh); % Count number of hydrophones
nsensora=length(isensora); % Count number of accelerometers
nfile1=length(ifilev1);
for inumber=ifilev1
    eval(['load pb450',num2str(inumber),'.'])
    dbbare=dbpower;
    dbbare=dbbare-cal-(dbbare(:,10)-cal(:,10))*ones(1,15); % remove force
    db1acc=dbbare(:,isensora);
    db1hyd=dbbare(:,isensorh);
    db1powerh=(10).^(db1hyd/10);
    db1powera=(10).^(db1acc/10);
    dbavgh=mean(db1powerh);
    dbavga=mean(db1powera);
    addbarehydpower=addbarehydpower+dbavgh;

```

```

        addbareaccpower=addbareaccpower+dbavga;
end
avgbarehydpower1=addbarehydpower/nfile1;
avgbareaccpower1=addbareaccpower/nfile1;
addbarehydpower=0;addbareaccpower=0;      %re-initialize value
ifilev2=[22:26];
isensorv2=[11:15];
nsensor2=length(isensorh);
nfile2=length(ifilev2);
for inumber=ifilev2
    eval(['load pb450',num2str(inumber),'.'])
    dbbare=dbpower;
    dbbare=dbbare-cal-(dbbare(:,10)-cal(:,10))*ones(1,15); % remove force
    db1acc=dbbare(:,isensora);
    db1hyd=dbbare(:,isensorv2);
    db1powera=(10).^(db1acc/10);
    db1powerh=(10).^(db1hyd/10);
    dbavgh=mean(db1powerh)';      %Average over 5 hydrophones
    dbavga=mean(db1powera)';
    addbarehydpower=addbarehydpower+dbavgh;
    addbareaccpower=addbareaccpower+dbavga;
end
avgbarehydpower2=addbarehydpower/nfile2;      %44 total hydrophone values
avgbarehydpower=avgbarehydpower1*(.716)+avgbarehydpower2*(.284);%weighted averages
avgbareaccpower2=addbareaccpower/nfile2;
avgbareaccpower=avgbareaccpower1+avgbareaccpower2;
dbbarehydpower=10*log10(avgbarehydpower);
dbbareaccpower=10*log10(avgbareaccpower);
bare450hyd=dbbarehydpower; %Used for XFER function graphs
bare450acc=dbbareaccpower; %Used for XFER function graphs
figure(1)
    clf
    hold on
    plot(fbin,dbbarehydpower)
figure(2)
    clf
    hold on
    plot(fbin,dbbareaccpower)
%
%-----Coated Analysis at 450 feet
% Runs PC4501 through PC45010 considered. All hydrophones used.Run 4502 bad.
path('c:\cylinder\data\bare50',path)
load pcal1
cal=dbpower;
path('c:\cylinder\data\coat450',path)
addcoathydpower=0;addcoataccpower=0;hsum=0;
ifilev3=[1 3 4 5 6 7 8 9 10];
nfile3=length(ifilev3);
for inumber=ifilev3
    eval(['load pc450',num2str(inumber),'.'])
    dbcoat=dbpower;
    dbcoat=dbcoat-cal-(dbcoat(:,10)-cal(:,10))*ones(1,15); % remove force
    db2hyd=dbcoat(:,11:15);
    db2acc=dbcoat(:,isensora);

```

```

db2powerh=(10).^(db2hyd/10);
db2powera=(10).^(db2acc/10);
dbavgh=mean(db2powerh)'; %
dbavga=mean(db2powera)';
addcoathydpower=addcoathydpower+dbavgh; %sum values for averaging
addcoataccpower=addcoataccpower+dbavga;
end
avgcoathydpower=addcoathydpower/nfile3;
avgcoataccpower=addcoataccpower/nfile3;
dbcoathydpower=10*log10(avgcoathydpower);
dbcoataccpower=10*log10(avgcoataccpower);
coat450hyd=dbcoathydpower;
coat450acc=dbcoataccpower;
figure(1)
plot(fbin,dbcoathydpower,'g-')
legend('Uncoated','Coated')
title('Hydrophone Response--Power avg, calibrated--450 Feet')
xlabel('Frequency'), % Freq Domain trace
ylabel('Level (dB)'), % Same with amplitude
axis([1 12000 -25 5])
grid on
figure(2)
plot(fbin,dbcoataccpower,'g-')
legend('Uncoated','Coated')
title('Accelerometer Response--Power avg, calibrated--450 Feet')
xlabel('Frequency'), % Freq Domain trace
ylabel('Level (dB)'), % Same with amplitude
axis([1 12000 -30 5])
grid on
figure(3)
clf
diffhyd=coat450hyd-bare450hyd;
plot(fbin,diffhyd)
title('Coating Effectiveness @ 450 Feet (CoatHd-BareHd)')
xlabel('Frequency'), % Freq Domain trace
ylabel('Level (dB)'), % Same with amplitude
axis([1 12000 -15 5])
grid on
figure(4)
clf
hold on
baretrans=bare450hyd-bare450acc;
coattrans=coat450hyd-coat450acc;
plot(fbin,baretrans)
plot(fbin,coattrans,'g-')
title('Bare & Coated Transfer Functions @ 450 Feet')
xlabel('Frequency'), % Freq Domain trace
ylabel('Level (dB)'), % Same with amplitude
legend('Uncoated','Coated')
axis([1 12000 -10 20])
grid on
figure(5)
clf
transfer=coat450hyd-bare450hyd-coat450acc+bare450acc;

```

```

plot(fbin,transfer)
title('Transfer Function @ 450 Feet (CoatHyd-BareHyd-(CoatAcc-BareAcc))')
xlabel('Frequency'), % Freq Domain trace
ylabel('Level (dB)'), % Same with amplitude
axis([1 12000 -10 20])
grid on

```

C. BDECAY3 -- This file was used to capture and display the 800 HZ decay sequence plotted in figure 2-5(b)

```

% BDECAY3---Time Capture Data and Convert
% Created by R. Meyer (MIT)
% File loads trace from time capture from HP-3563A
% File captures response of 800 hz signal to cylinder
% Operator needs to check/clip first couple of points
% using Word 6.0. Also input 1/2 peak voltage and time
% length of the display (in msec).
% Use VBLK8 and DVAS sequence to aquire data.
% Date:18 Apr 97
clf
path('c:\gpib95',path)
fid=fopen('BDEC3.DAT');
a=fscanf(fid,'%g',[1 inf]); % create a column for volts
b=1:length(a); % create row for time calc
c=b'; % transpose creates time col
% calibration data (from HP-3563A)
volthigh=.240535; %Off HP-3563A max voltage
voltage=-.24669; %Off HP-3563A min voltage
voltscale=volthigh-voltage; %P-P mvolts (AC) span
voffset=150; %Use time offset only if you zoom
%in on a time capture w/3563
timescale=200; %time measured in msec
%For DVAS (use screen limits)
%For DDAS (time for all records)

vrange=max(a)-min(a); %voltage range (not normalized)
voltsa=a-min(a); %move data points to touch axis
voltsb=voltsa-vrange/2; %plot on either side of axis
voltcal=voltscale/vrange; %calibrate the data points
volts=voltsb.*voltcal; %normalized voltage values
samplerate=256000; %sample frequency is 256 kHz
%
%Message time in a similar manner
timecal=timescale/length(a);
time=c.*timecal+voffset; %normalized time values
%Atime=[164:340]'
%least=.245+.0003389*.Atime
% First plot shows signal prior to source removal
hold on
subplot(2,1,1),plot(time,volts)
grid
axis([160 200 -.25 .25])
xlabel('msec'), % Should match 3563A trace

```

```
ylabel('volts'),          % Amplitude requires p-p values
```

```
% Note oscillations produced for 800 hz curve
```

```
subplot(2,1,2),plot(time,volts)
```

```
axis([160 300 -.25 .25])
```

```
xlabel('msec'),          % Should match 3563A trace
```

```
ylabel('volts'),          % Amplitude requires p-p values
```

```
grid
```

```
hold off
```